

Construction of Precision sMDT Detector for the ATLAS Muon Spectrometer Upgrade

D. Amidei^a N. Anderson^{a,1} A. Chen^a E. Carpenter^a L. Cooperrider^a T. Dai^a E. Diehl^a C. Ferretti^{a,1} Y. Guo^a J. Li^{a,c} X. Meng^a K. Nelson^a V. Pillsbury^a E. Salzer^a T. Schwarz^a L. Simpson^a Z. Wang^a C. Weaverdyck^a C. Wei^{a,b} Z. Yang^{a,b} M. Yuan^a B. Zhou^a J. Zhu^a

^a*Department of Physics, University of Michigan, 450 Church Street, Ann Arbor, MI 48109, USA*

^b*Department of Modern Physics, University of Science and Technology (USTC), 96, JinZhai Road Baohe District, Hefei, Anhui, 230026, China*

^c*Physics Department, Shanghai Jiao-Tong University, 800 Dongchuan Road, Minhang, Shanghai, China*

E-mail: claudio.ferretti@cern.ch, [Contact Editor](#)

ABSTRACT:

This paper describes the small-diameter monitored drift-tube detector construction at the University of Michigan as a contribution to the ATLAS Muon Spectrometer upgrade for the high-luminosity Large Hadron Collider at CERN. Measurements of the first 30 chambers built at Michigan show that the drift tube wire position accuracy meets the specification of $20\ \mu\text{m}$. The positions of the platforms for alignment and magnetic field sensors are all installed well within the required precision. The cosmic ray test measurements show single wire tracking resolution of $100 \pm 7\ \mu\text{m}$ with an average detection efficiency above 99%. The infrastructure, tooling, techniques, and procedures for chamber production are described in detail. The results from the chamber quality control tests of the first 30 constructed chambers are reported.

Contents

1	Introduction	2
2	Infrastructure and Tooling for sMDT Construction and Testing	4
2.1	High bay and large granite table	4
2.2	Automatic glue machine	4
2.3	Precision combs	5
2.3.1	Precision jiggling survey and setup on granite table	6
2.3.2	Measured precision of the combs	8
2.4	Spacer frame assembly jiggling and in-plane alignment system	10
2.5	Survey of the jiggling for sensor platform installation	12
2.6	Chamber test stations	13
2.6.1	Chamber service installation and leak test station	13
2.6.2	Cosmic ray test station	14
3	sMDT Base Chamber Construction on Granite Table	15
3.1	Spacer frame and in-plane alignment system assembly	15
3.2	Gluing an sMDT base chamber	16
3.3	Installation of the platforms and the chamber supporting structure	17
3.4	Measurements of the base chamber mechanical precision	19
3.4.1	Platform position measurements	19
3.4.2	Tube position measurements	20
3.4.3	Chamber shape deformation measurements	22
4	Chamber Services Installation and Testing	22
4.1	Gas-bar assembly, cleaning, and installation on chamber	23
4.2	Front-end electronics installation	24
4.3	Chamber gas tightness measurement	25
4.4	Ground cable connections	27
5	Electronics and Cosmic Ray Test	27
5.1	Noise rate measurements	28
5.2	Tube spectra from cosmic ray data	29
5.3	Tube and chamber efficiencies	29
5.4	Tracking resolution	31
6	Database	32
7	Conclusion	33

1 Introduction

The ATLAS Muon Spectrometer (MS) is the largest muon spectrometer ever constructed [1]. Currently in the barrel (pseudo-rapidity $|\eta| < 1.05$) Resistive Plate Chambers (RPC) provide fast timing trigger-signals to identify events containing muons and Monitored Drift-Tube (MDT) chambers provide precision tracking. In the end-cap ($1.05 < |\eta| < 2.7$) the muon trigger comes from Thin Gap Chambers (TGC) and precision tracking from MDTs and in the innermost region the new Small-Wheel [2] (consisting of MicroMegas and small-gap TGC detectors). The barrel contains 20 layers of MDTs in three concentric stations, each with a single tube resolution of $80 \mu\text{m}$, plus 3 stations of RPCs on the middle and outer MDT stations. The MDTs are arranged in 16 sectors around the beam line, covering 2π in alternating "large" and "small" chamber sizes, referred to as "Large" and "Small" sectors. The ATLAS MS will be upgraded [3], scheduled in 2026-28, for the high-luminosity LHC (HL-LHC) operations. One major MS upgrade project is to add an extra triplet-station of small-gap RPC (sRPC) chambers to the barrel inner MS station to improve the muon Level-1 trigger efficiency. To accommodate the new sRPCs, the MDTs of 8 Barrel-Inner-Small (BIS) sectors will be replaced with small-diameter (15 mm) MDTs (sMDT's) designed and developed by the Max Planck Institute (MPI) [4], which are half of the thickness of the MDTs. The 8 Large sectors have space for inserting the new sRPCs, so the current MDTs will

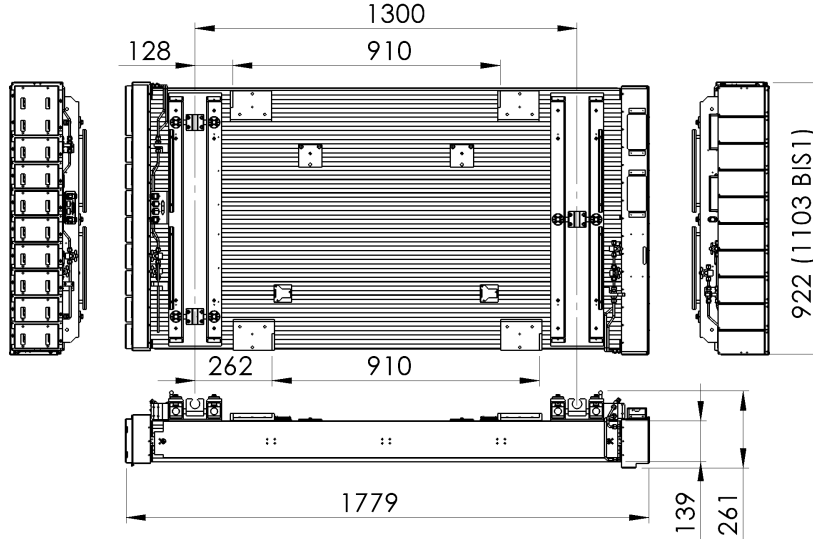


Figure 1: Drawing of a BIS2 sMDT chamber. Quoted dimensions are in mm.

remain. MPI and the University of Michigan (UM) are sharing equally the production of a total of 100 sMDT chambers. An sMDT chamber consists of 2 tube multi-layers (ML), each containing 4 tube layers of 70 (BIS1) or 58 (BIS2-6) tubes. The geometry of a BIS2 is shown in figure 1, while figure 2 shows a complete BIS4 chamber built at UM.

For the US site, the tubes are constructed and tested at Michigan State University (MSU), then shipped to UM, where they are fully retested [5] before chamber construction. A spacer frame (parts made at IHEP¹), containing the RASNIK in-plane alignment system [6] (from NIHKEF²), is glued between the two ML's. Platforms (from Saclay³) for mounting the magnetic field sensors and global alignment devices [7] are glued on top of the chamber, together with the chamber kinematic mounts on supporting structures (from IHEP). Temperature sensors assembled with cables (from NIHKEF) are distributed on both ML's. The Faraday cages (from IHEP) cover the front-end electronics (from LMU⁴) with 2 HV distribution boxes (from MPI) mounted on top of them.

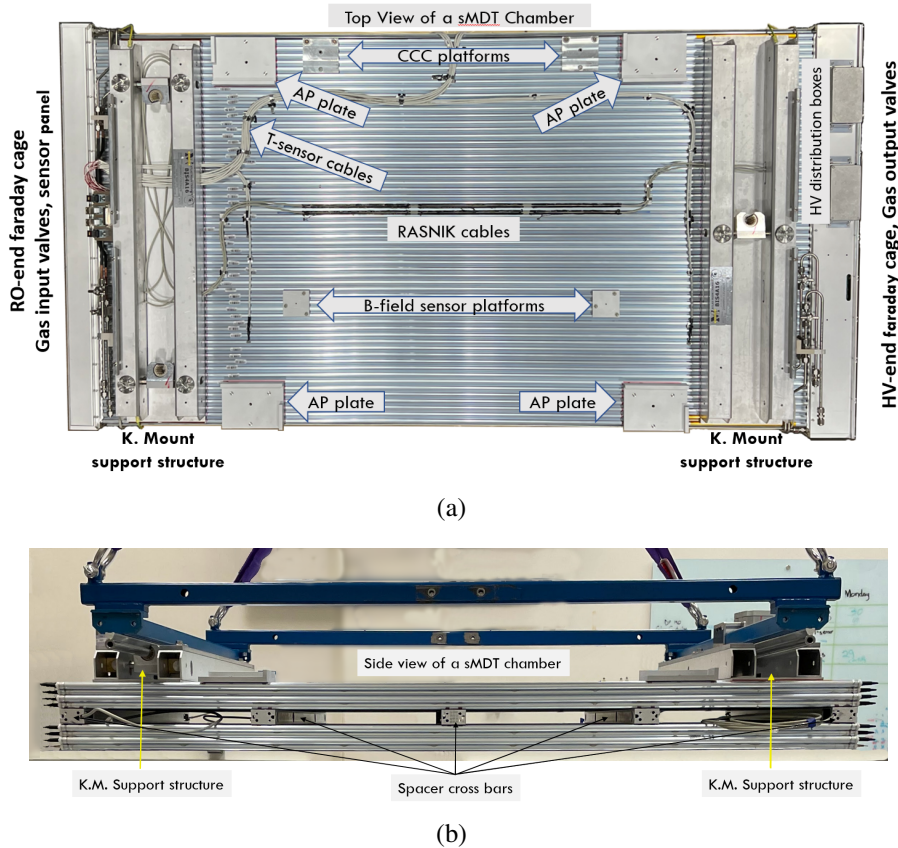


Figure 2: Chamber view: a) *top* with platforms, support structures, temperature cable routing, sensors readout panel, gas pipes, Faraday cages, and HV splitter boxes. CCC and AP platforms are intended for the global alignment sensors; b) *side* with kinematic mounts on the support structures holding the chamber to a overhead crane. The spacer bars are visible between the two ML's.

This paper reports the sMDT chamber construction infrastructure, assembly procedure, quality control, and performance test results at UM.

¹Institute for High Energy Physics, Protvino, Russia

²National Institute for Subatomic Physics, Amsterdam, Netherlands

³Saclay Nuclear Research Centre, Saclay, France

⁴Ludwig Maximilian University, Munich, Germany

2 Infrastructure and Tooling for sMDT Construction and Testing

From 2017 to 2020 UM built the infrastructure for sMDT chamber construction as well as two prototype precision sMDT chambers to certify the tooling and chamber assembly procedures. The mass production of the sMDT chambers at UM started in April 2021. The sMDT chamber construction infrastructure and tooling are described in this section.

2.1 High bay and large granite table

The chamber construction makes use of 2 large ($20 \times 20 \text{ m}^2$) high bay research labs (see figure 3(a)) in the UM physics building. These are equipped with multiple overhead cranes and a clean room portion outfitted with a $3 \times 7 \text{ m}^2$ granite table with 25 micron flatness. This clean room utilizes a dedicated HVAC system to maintain $\pm 0.5^\circ\text{C}$ temperature stability and $\pm 5\%$ humidity stability. The chamber parts (tubes, structural elements and platforms) are assembled on the granite table using precision jigging and glued together using an automated epoxy dispensing machine.

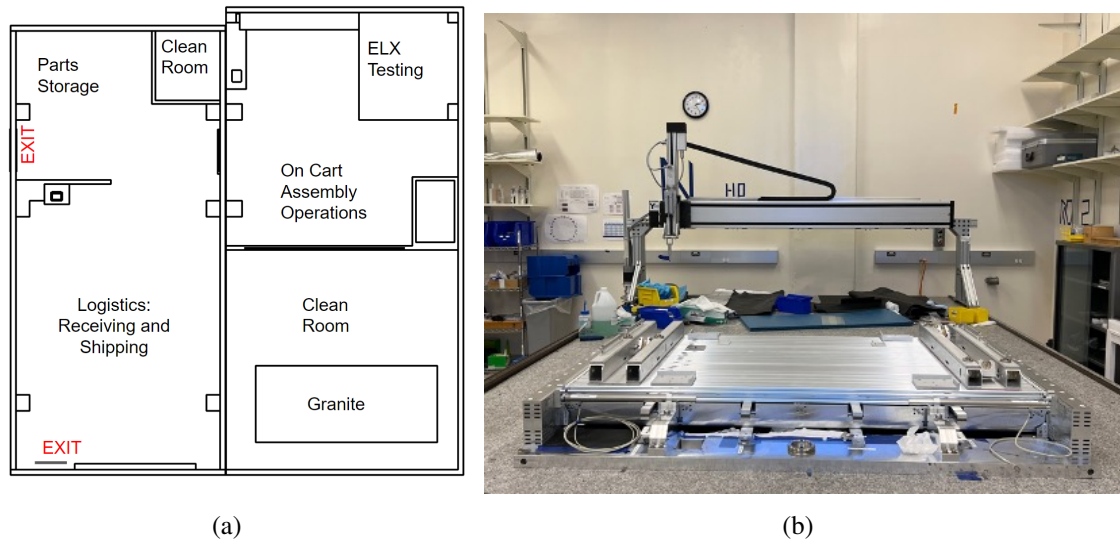


Figure 3: (a) Map of the sMDT construction labs in the high bay area. (b) The glue-machine and a constructed sMDT chamber on the granite table in the temperature and humidity controlled room.

Installation of the chamber's gas system and front-end electronics is done after the chamber is moved to mobile stations in the space outside the clean room.

A sub-room in the corner (labeled as "ELX Testing" in the room map) was built to keep the humidity below 40% for chamber cosmic ray testing. Another bay-area is used for storing and shipping chambers as it has two overhead cranes and a roll up outside door for loading chambers into a shipping container. A small clean room in this bay area is used for clean parts storage and gas-bar pre-assembly.

2.2 Automatic glue machine

A large gantry-mounted, computer driven glue dispensing machine was designed and built at UM. It controls the 3D motion (marked X, Y, and Z on the machine) of the dispensing tip as well as

the drive piston for the epoxy cartridge (A drive). The gantry is assembled from $7.6\text{cm} \times 15.2\text{cm}$ aluminum extrusions which ride on carriages on rails mounted directly on the surface of the granite table (see figure 4(a)). The two rails on the granite are aligned to be parallel within 7 micro-radians.

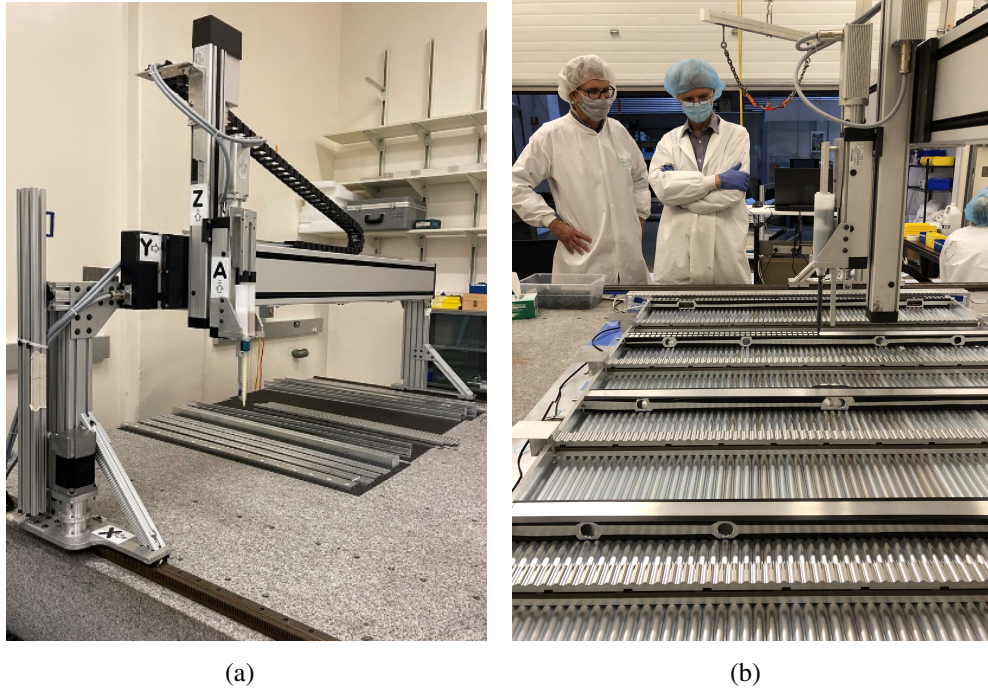


Figure 4: (a) Four motion actuators for 3D motion of the glue dispenser, all computer-controlled. (b) Gluing the spacer frame on the bottom multi-layer of a chamber.

The X drive engages a toothed rail on one side of the granite, which moves the gantry along the long dimension of the table with a precision of 0.1 mm. The linear rail carriages and rail are kept clean and lubricated to minimize frictional drag. The Y, Z, and A drives are linear actuators⁵. The gantry Y axis, with a range of 2.5 m, travels along the length of the tubes (see figure 4(b)). The actuator along the Z axis has a range of 0.5 m to allow the movement of the gluing cartridge over the whole vertical dimension of a chamber, from the first layer to the supporting structures at the top. The A drive expels epoxy from the cartridge and is programmed to move in steps of 0.26 mm to dispense 0.5 cc epoxy at a time. The control software is written with LabView[8] which interfaces with the motor drivers provided by the manufacturers. Specific sequences of gantry motions and epoxy dispensed at each location on the gantry path are designed and tested to determine the configurations used for gluing each tube layer, spacer frame, and support structure.

2.3 Precision combs

The precision combs are the jigging used to precisely position tubes for chamber construction and were designed by MPI and made in Germany for both production sites. Combs are used on both the chamber readout (RO) and high voltage (HV) ends. Each endplug has a precision brass surface of diameter $5.00^{+0.00}_{-0.01}$ mm which is concentric to the tube-center (therefore to the wire) within

⁵<https://www.isel.com/en/linear-units-les4.html>, and <https://www.isel.com/en/linear-units-les5.html>

5 microns rms. The endplug precision surface is captured between two half-holes in adjacent stacked combs. A full comb set consists of 9 stacked plates with precision holes (paired half-holes) of diameter $5.00^{+0.01}_{-0.00}$ mm on the interfaces between adjacent plates (see fig 5(a)). Each plate is fixed to the one underneath with 17 screws tightened to 7.5 Nm torque. The base comb is 50 mm thick for rigidity and subsequent combs are 13.077 mm thick except for a 45.600 mm thick comb which sets the gap for the spacer frame.

The combs locate the tubes on a 15.100 mm horizontal pitch, and a vertical pitch (tube layer) of 13.077 mm. During assembly of the tubes into a chamber, the precision cylinder of each tube's endplugs are placed in the two end-combs as shown in figure 5(b). The lower comb's half-cylinders constrain the horizontal locations of the tubes' precision cylinders. The upper comb is screwed to the lower comb to provide a vertical constraint on tube position.

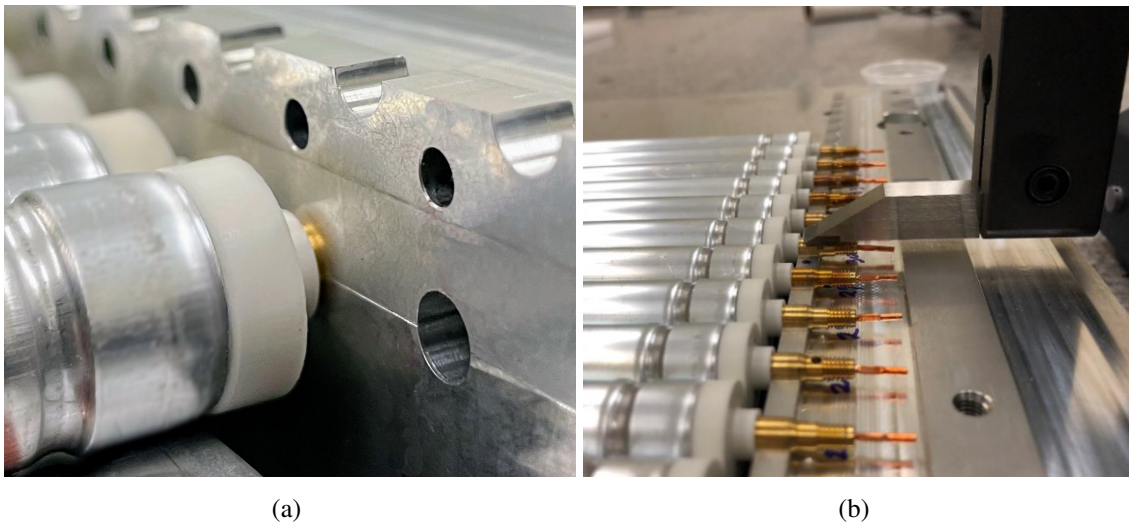


Figure 5: (a) Upper and lower combs constrain the location of the endplugs with high precision. The smaller holes at the top of the picture allow insertion of ground anchors which are screwed into the gaps between tubes after the epoxy has cured; (b) Tubes placed in the chamber construction combs. The heights of the endplug precision cylinders are measured using a height gauge.

Besides four base middle combs fixed to the table shown in figure 6(b), there is another set of four temporary combs used on top of the bottom ML when gluing the fifth tube layer on the spacer frame bars. These temporary combs replace the four middle combs on the granite which are not accessible when gluing the top ML. In addition there is a set of four weights with 7.5 mm radius semi-circles cut in the bottom surface which are placed on top of each freshly glued tube layer to control the straightness and potential bowing of the tubes.

2.3.1 Precision jiggling survey and setup on granite table

The set up of the combs on the granite was an iterative process, alternating between adjusting the jiggling positions and making precision measurements of the jiggling. Positions were measured

with both a FARO-arm⁶ for 3D-measurements with precision of 10 μm and a height gauge⁷ for measuring height relative to the granite table surface with a precision of 5 μm . Figure 6(a) shows the two base precision end-combs which are bolted at opposite ends of two crossbars. The RO comb is in the foreground and the height gauge is visible measuring the HV comb at the far side of the table. The middle base-combs, shown in figure 6(b), are connected to the two cross-bars and ensure tube straightness when tubes are glued. The middle base-combs are aligned both along the tube direction (yellow-dashed lines in figure 6(b)) and in height to better than 50 μm using the FARO-arm.

Each end comb base is clamped onto the granite table at two points using 100 microns precision shims under the combs. The combs are also bolted to heavy side bars which set the length of the jiggging. The base combs need to be set parallel to each other and perpendicular to the wire direction. The wire direction must be aligned with the glue machine Y axis and this alignment is periodically verified and the Y gantry position tuned if necessary.

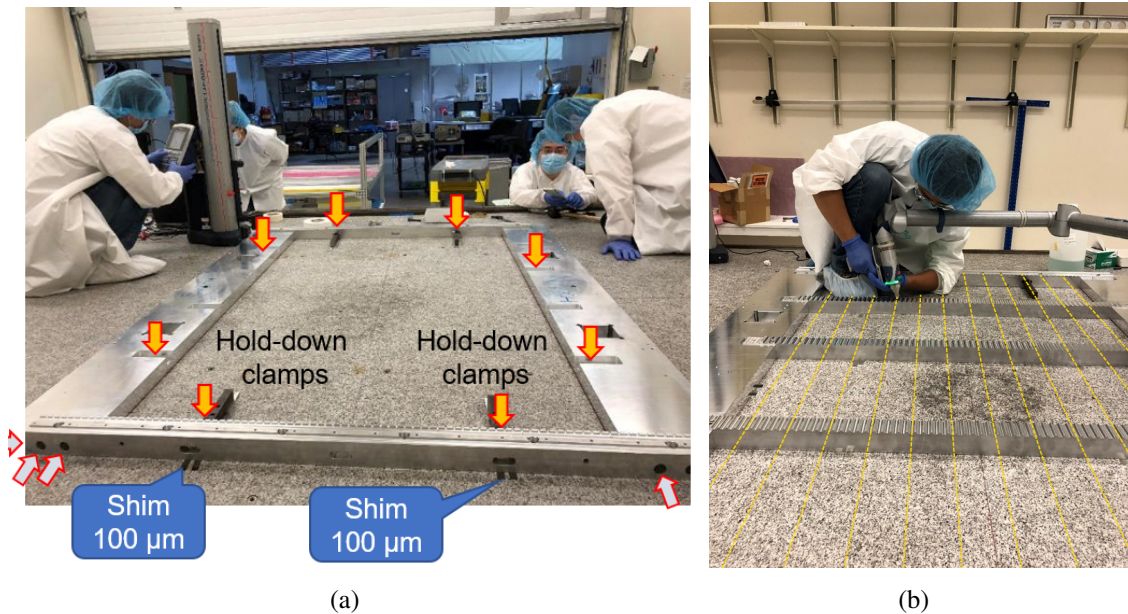


Figure 6: Set up of base and mid-combs: (a) the two precision base end-combs are connected to two sidebars by bolts indicated by the white/red arrows. The yellow/red arrows point to the hold-down clamps of the base jigging; (b) the middle base-combs are connected to the two sidebars.

The squareness of the base-comb setup was checked using the Faro-arm to measure the diagonals defined by precision half-circular cylinders placed on comb notches 4 and 67 (as in figure 9(a)). These diagonals differ by 15 microns from the average and the angles between the comb assembly and the long base-plates have a maximum deviation of $0.0018^\circ = 0.03 \text{ mrad}$ from 90° , as shown in figure 7.

⁶<https://www.faro.com/en/Resource-Library/Tech-Sheet/techsheet-8-axis-edge-faroarm-scanarm>

⁷https://www.mitutoyo.com/webfoo/wp-content/uploads/2104_LH-600E.pdf

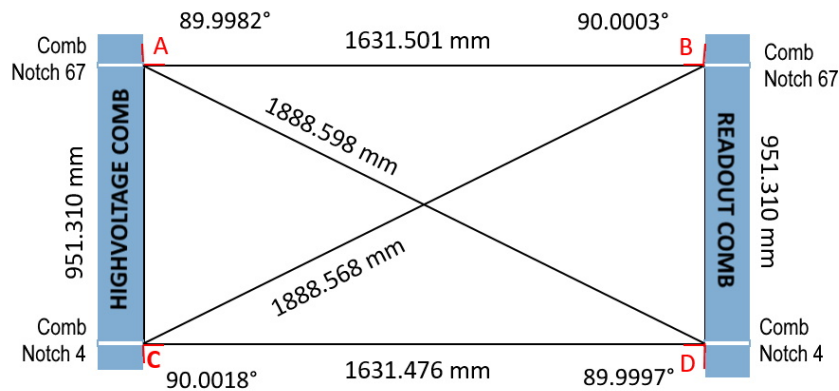


Figure 7: Base comb layout geometry and measured distances and angles.

2.3.2 Measured precision of the combs

As mentioned previously, there are two sets of precision combs, one for the chamber RO-end and the other for the HV-end. Figure 8 shows one set of the combs stacked on the granite table. The comb geometry precision was measured three ways: comb flatness, and the horizontal and vertical pitches of the tube positions defined by the holes in the combs.

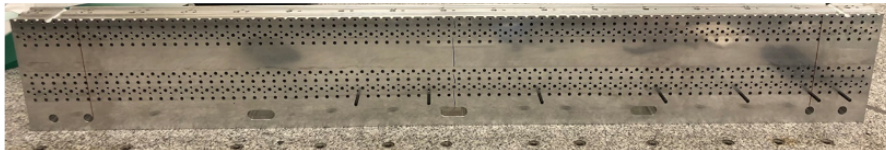


Figure 8: One set of the precision combs stacked on the granite table.

The flatness of the base-combs was measured with the height gauge using precision rods placed in the combs precision half-circles (see figure 9(a)). Both base combs, when first set up on the granite, had a bowed shape, where the ends were about 80 microns higher than the middle. This same shape was seen in subsequent layers as they were added to the base comb. Flattening of the base combs was achieved by an iterative process of loosening the screws holding the ends of the base to the side bars, applying downward pressure on the outer ends and re-tightening the screws followed by height measurements, and repeating the whole process until the combs were sufficiently flat. The measured shapes after the flatness tuning of the readout (RO) and high voltage (HV) side base combs are shown in figure 10 (green data-points). The measured standard deviation (RMS) of the comb flatness is smaller than 10 μm for both base-combs. The initial indexed tube locations above 60 show higher deviations, at the level of 20 microns. After the construction of the first twelve SMDT chambers, the RO and HV base comb shapes were re-flattened using the method described above. The blue data-points in figure 10. show and improvement of the average flatness to 1 μm or better and of the RMS from 9 μm to 5 μm .

The Faro-arm with a precision spherical probe tip was used to measure the half-cylinder center positions on the combs to determine the wire pitch (see figure 9(b)). Measurements of the

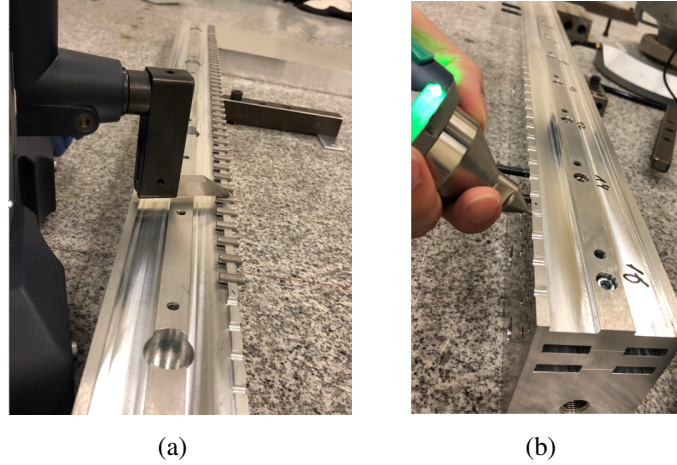


Figure 9: Precision comb geometry measurements: (a) flatness using the height gauge; (b) wire pitch using the FARO-arm to determine the center positions of the comb half-cylinders.

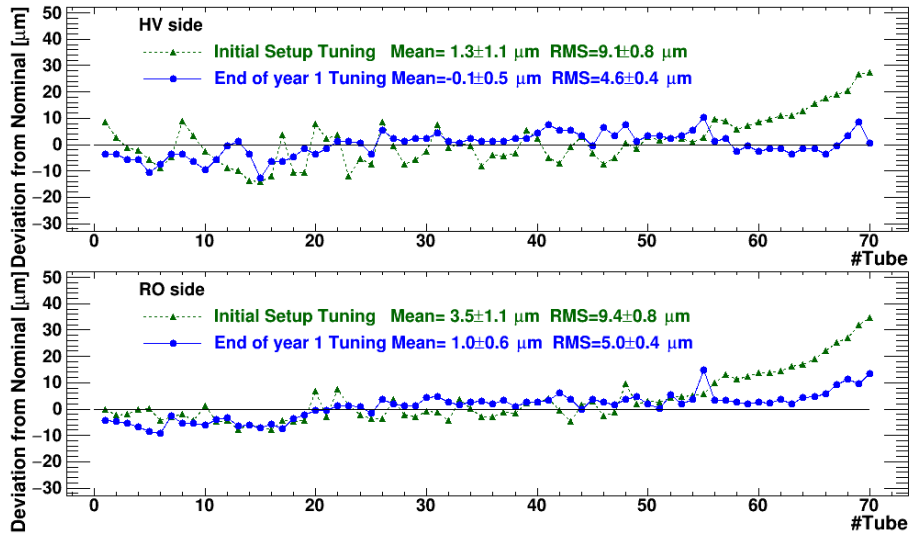


Figure 10: Base comb cylinder center height measurements relative to the target wire height above the granite surface for HV and RO sides, showing the initial tuning and the re-tuning after assembly of the 12th chamber.

deviations of the base comb cylinder center pitch (wire pitch) from the nominal value (15.100 mm) are shown in figure 11. The horizontal wire pitch were measured to be 15.1017 ± 0.0005 mm (15.1019 ± 0.0004 mm) for the RO (HV) comb, with an RMS of about 4 microns.

The complete geometry of the vertical-pitch (tube layer pitch) on both RO and HV sides was measured on the granite table with 5 microns precision using the height gauge and shown in figure 12. The tube layer pitch was measured to be 13.077 ± 0.005 mm (13.076 ± 0.005 mm) and the spacer frame height 45.604 ± 0.005 mm (45.599 ± 0.005 mm) for the HV (RO) side.

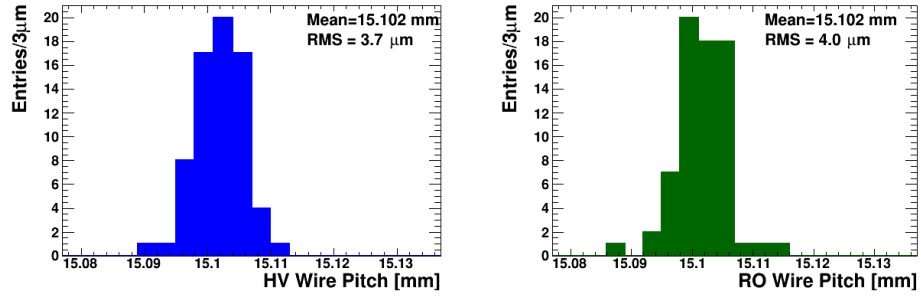


Figure 11: Measurements of the base-comb wire pitch, for both HV and RO side.

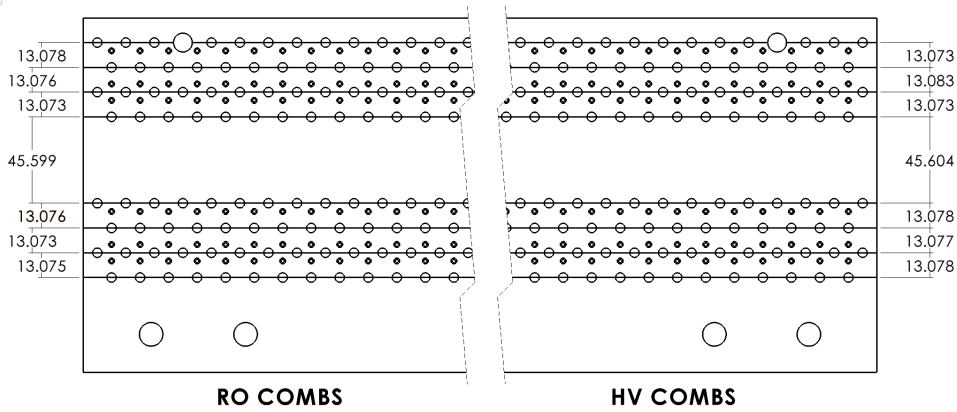


Figure 12: Summary of the measured precision comb vertical tube-pitch, for both RO and HV side after set up on granite table. Values are in mm.

2.4 Spacer frame assembly jiggling and in-plane alignment system

The spacer frame consists of five aluminum extrusions with rectangular cross-sections of dimensions $880 \times 30 \times 50 \text{ mm}^3$. The in-plane optical devices are housed inside the spacer frame cross-bars as shown in figure 13(a). The bars and two side support panels are assembled using the jiggling shown in figure 13(b). Precision end blocks are glued to the ends of the cross-bars and bolted to two side-plates to form a rigid frame. The side panels are needed to preserve the relative positions of the cross-bars before the spacer frame cross-bars are glued onto a ML and are removed at the end chamber assembly.

The spacer frame jiggling consists of two rigid aluminum L-shaped bars firmly bolted to the table at right angles. The angle between them was set using FARO-arm measurements. The jiggling bars are machined with cutouts to match the side panel profile and several L-shaped brackets are mounted on them to reinforce the clamping. One side-panel and one cross-bar are clamped to the jiggling during the assembly process to ensure the flatness and perfect rectangular shape of the frame while the glue is curing.

The in-plane alignment system consists of 4 RASNIK lines, 2 diagonal, and 2 straight, along the sides of the chamber. The RASNIK system is a three-point system (coded mask, lens, CCD) that is sensitive to the relative movement of any of the three elements. A schematic of a RASNIK system with readout system (provided by NIKHEF and customized at UM as part of the chamber

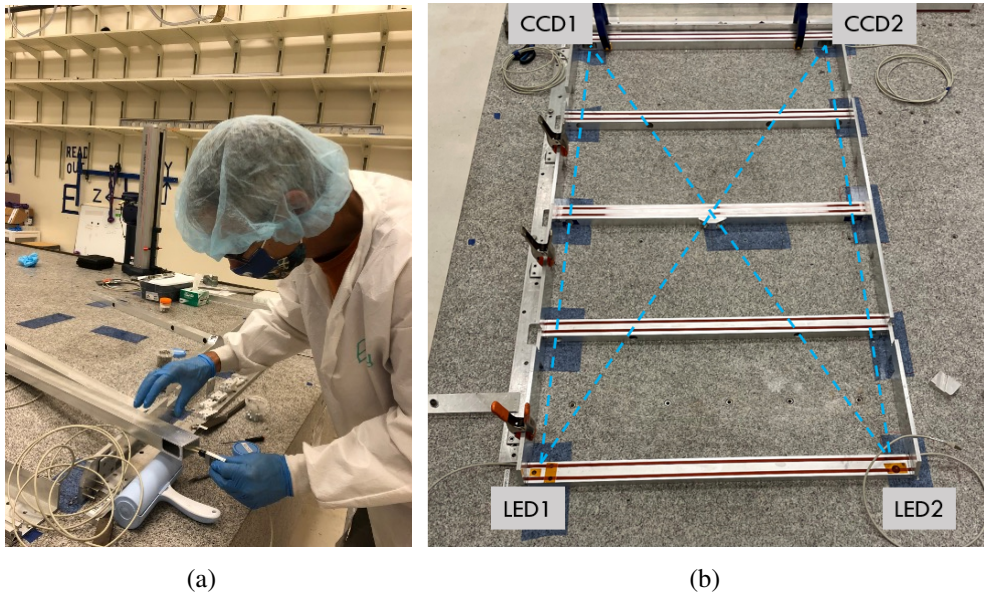


Figure 13: (a) Assembly of the in-plane system parts into the cross-bar; (b) spacer frame assembling with a jiggging setup on the granite table. The locations of the in-plane devices, LEDs and CCDs, inside the cross bars are indicated as well as the four RASNIK lines, (blue lines).

assembly tooling) is shown in figure 14. The coded mask is back-illuminated by an LED and imaged with a lens onto a CCD. Analysis of the image of the coded mask reveals displacements transverse to the surface of the mask accurate to 1 micron.

The in-plane system has 2 LED-Masks and 2 CCDs. Each CCD views sequentially images of each LED-Mask to provide one straight and one diagonal measurement. Reference RASNIK measurements are taken after chamber assembly on the granite table when the chamber is considered to be in perfect alignment while still held by the precision jiggging. RASNIK measurements taken after the chamber is moved from the granite reveal chamber deformations when subtracted from the granite reference RASNIK measurements.

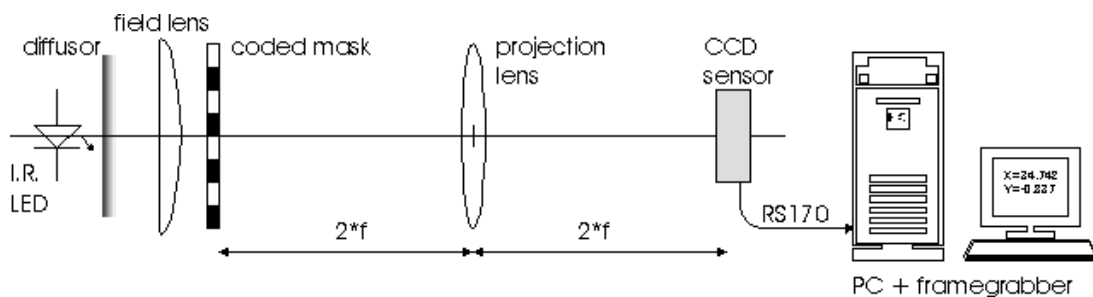


Figure 14: RASNIK system showing LED illuminating a coded mask on left, imaging lens in the center, and CCD on the right. The CCD image is read out and analysed by a computer.

2.5 Survey of the jiggging for sensor platform installation

Two different jiggging sets (one for BIS1 and another for BIS2-6 chambers), provided by MPI, are used to install the sensor platforms on top of each chamber while it is still on the combs, so that the platform locations can be set and measured with precision. The combs determine the geometric grid of wires within a chamber. Knowledge of where one chamber's wires are relative to its neighbors in the same plane is provided by a set of Axial-Praxial (AP) sensors. The exact locations of 3 planes of each AP platform relative to the wire grid must be accurate within 0.20 mm and known to within 0.03 mm. Furthermore each chamber has two Hall sensors (for measuring local magnetic field direction and intensity) and some chambers have CCC (Chamber to Chamber Connection) sensors for measuring a small (large) chamber's location relative to chambers in the adjacent large (small) sector. The AP platforms and CCC platforms must be glued with X, Y and Z positions accuracy each better than 200 microns compared to nominal designed positions. The precision on the measured 3D-positions are each required to be within 30 microns when referenced to the granite surface (Y-axis), endplug surface (X-axis), and the first wires on both sides of the chamber (Z-axis). The B-sensor platforms must be glued with positions better than 500 microns compared to nominal designed positions.

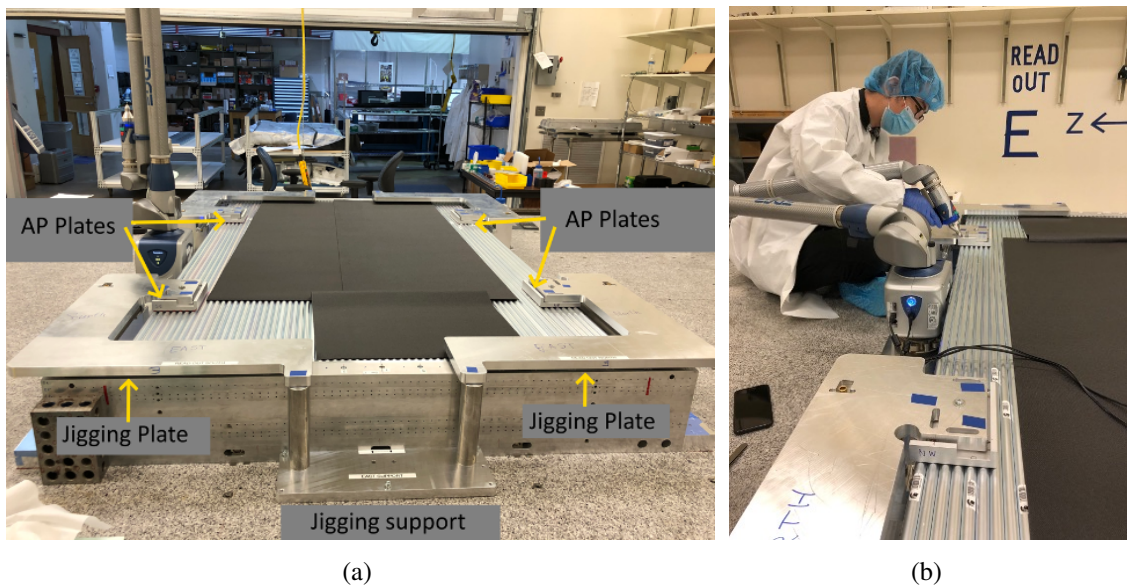


Figure 15: (a) Four AP plates on the top corners of a SMDT chamber, each held by a screw to a L-shaped jiggging; (b) a FARO-arm probe is used to check and adjust locations of AP platforms before and after gluing. Final positions are measured after glue is cured.

The AP jiggging references the comb precision holes to set each AP platform within 40 microns of a reference location. The AP jiggging supporting structures, two close to the end-combs and four mounted on the base cross bars, are tuned and measured so that all the surfaces of the L-shaped jiggging are parallel to the surface of the granite table. Each L-shaped jiggging (see figure 15(a)) holds one platform and allows fine 3D adjustments to be made via 6 contact points, two referenced to the first wire, one relative to the tube RO endplug surface and three to the surface of the granite

table. Each AP-plate's position is verified by FARO-arm measurements as shown in figure 15(b) before and after gluing.

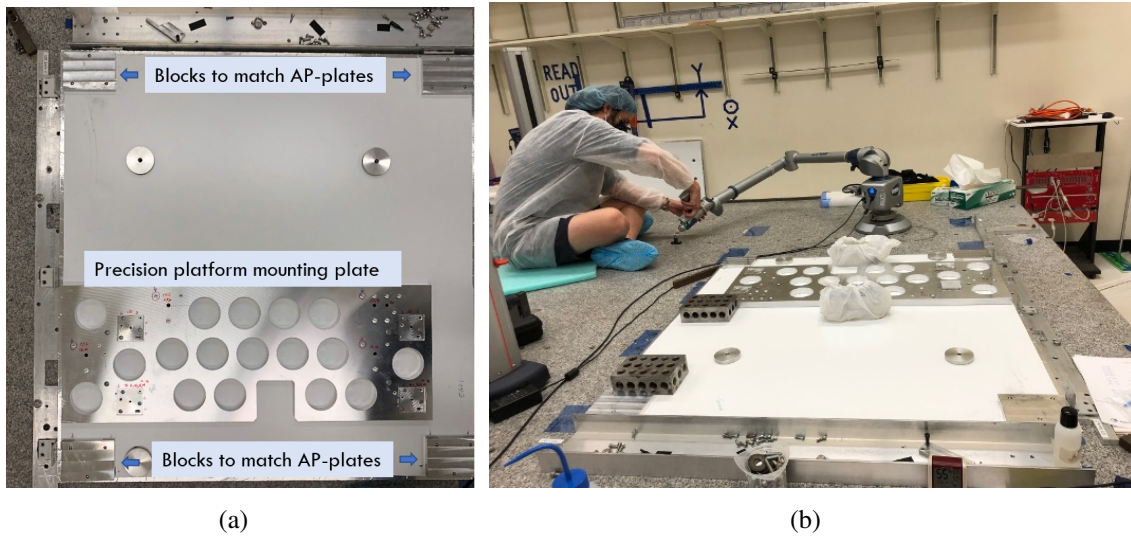


Figure 16: (a) Assembly plate to mount the B-field and CCC platforms for installation on chamber; (b) survey of the big plate with the FARO-arm.

The CCC-plates and B-sensor plates are mounted on a big precision plate where their positions are fixed relative to four blocks matching the AP-plate positions on the chamber (see figure 16(a)). Surveys on two assembly plates (for BIS1 and BIS2-6 chambers) were done using the FARO-arm on the granite table (see figure 16(b)). Mistakes were found on both of them. One was fixed by removing one of the four blocks and re-gluing it on the correct position on the plate. The other plate was rectified by gluing a 120 microns shim to the reference block which sets the X position of the platforms on the chamber, thus correcting the relative position of the platforms respect to the block. All the fixes were further verified by dry runs of installation of the platforms on a chamber.

2.6 Chamber test stations

Two chamber test stations were designed and built at UM. One is used for installation of on-chamber services (temperature sensors, cables, on-chamber gas system, temperature and RASNIK readout panel, HV and RO electronics hedgehog cards⁸, and Faraday cages) and for performing a gas tightness test. The other test station is dedicated to electronics and cosmic ray tests.

2.6.1 Chamber service installation and leak test station

The chamber services installation is done by mounting the chamber on a rotation cart consisting of a chamber-frame (provided by Protvino) mounted on rotation bearings on a movable base (figure 17 (a)). The chamber is attached to the frame using the chamber kinematic mounts. On the cart the chamber can be rotated through 360° on the base allowing easy access of all parts of the chamber, for example, when gluing temperature cables on top and bottom of the chamber. Two removable small

⁸Hedgehog cards are front-end electronics cards which attach directly to the tube endplugs.

tables can be connected to the chamber-frame for services installation tooling and parts. The rotation feature is also used to do a test of the in-plane alignment system by taking RASNIK measurements at different rotation angles and checking for a characteristic set of deflection measurements. Chamber ground cables, front-end hedgehog cards and Faraday cage installations on chambers are carried out in this station. An end-view of a chamber mounted on the rotation cart is shown in figure 17(b), where one gas-bar is installed on the bottom ML of the chamber, and one gas-bar is on the small table ready to be installed.

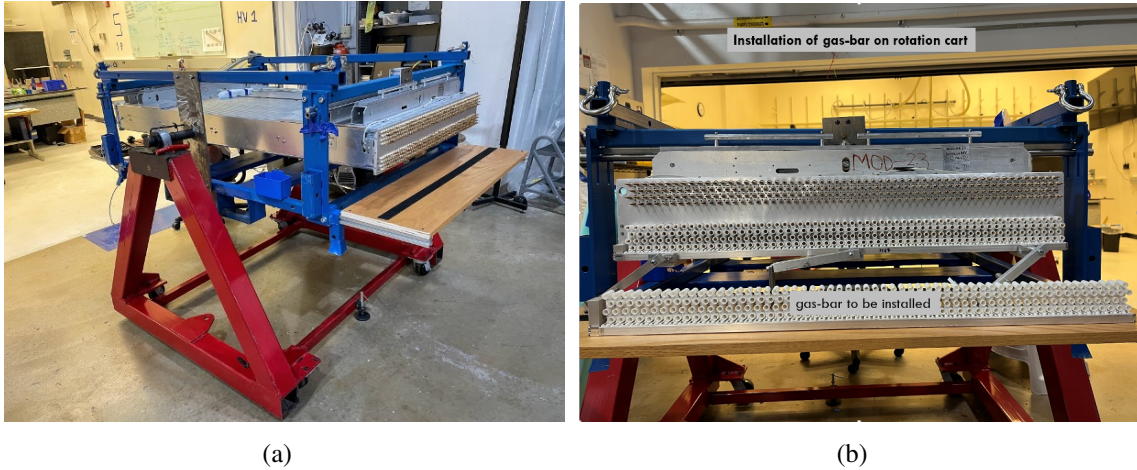


Figure 17: (a) A rotation cart for chamber service installation and testing; (b) Installation of the gas-bars on the rotation cart.

2.6.2 Cosmic ray test station

The chamber cosmic ray testing is performed inside a room where humidity is kept below 40%. The station itself consists of a scintillator trigger system mounted in a movable frame, a chamber cart with a gas control panel, HV/LV power supplies, and a data acquisition (DAQ) system [9]. The schematics of the cosmic ray test system, including an sMDT chamber, trigger detector, front-end electronics, the DAQ modules and data flow, is shown in figure 18.

Figure 19 (a) shows an sMDT chamber on the mobile cart with the scintillator ($1.2 \times 0.6 \text{ m}^2$) placed on top to provide fast trigger signal for the cosmic ray test.

The DAQ system (see figure 19(b)) is located outside the humidity-controlled chamber test room and consists of two computers (a Windows computer for DAQ configuration and controls and a linux computer for data-taking), a VME crate containing the DAQ interface and trigger modules, HV power supplies for chamber and for the trigger scintillator, and a NIM crate containing the trigger coincidence modules. The firmware of the DAQ and the software for online data monitoring were developed at Michigan. During the cosmic ray test the muon tracks, hit map, and the ADC and TDC spectra for each sMDT tube are displayed online, as shown in figure 19(b).

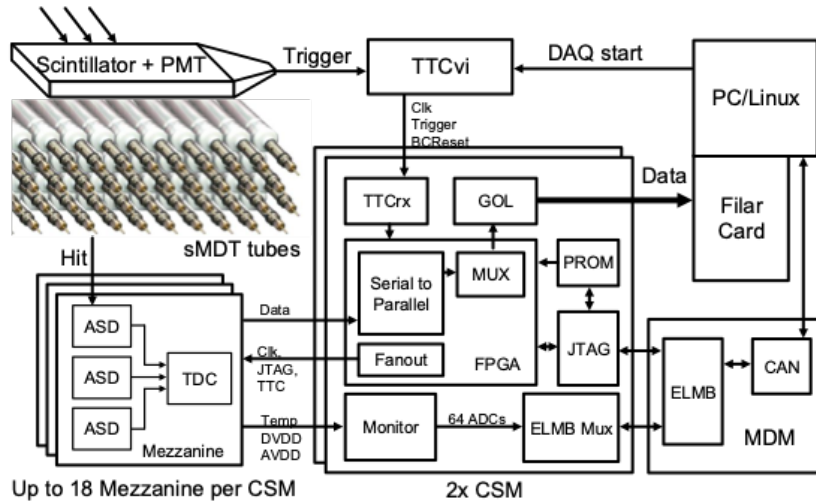


Figure 18: Block diagram of the sMDT readout electronics and the DAQ system.

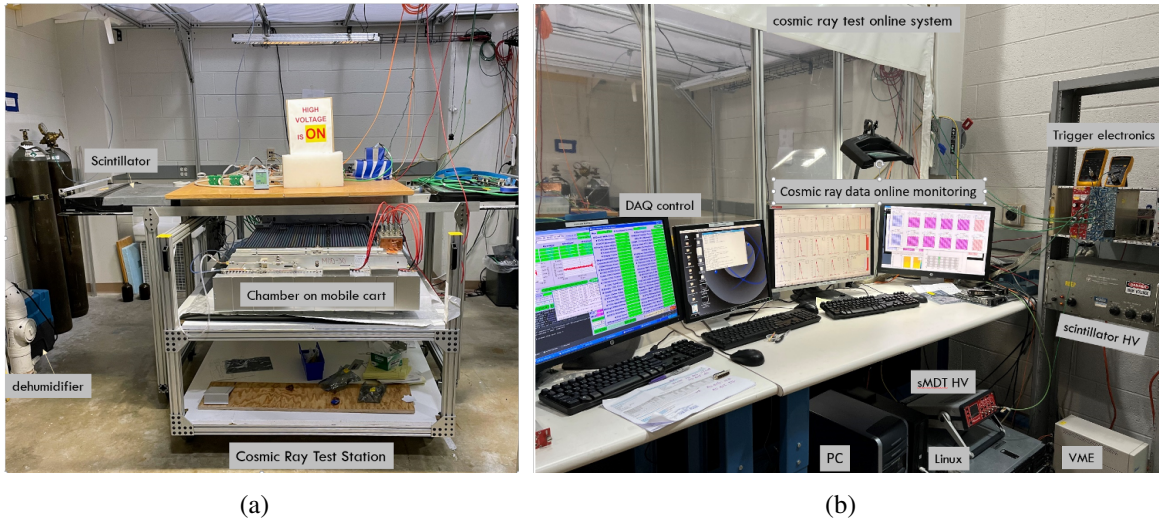


Figure 19: (a) Scintillation pad on a mobile support over a test chamber on a mobile cart connected with gas and HV; (b) online DAQ and monitoring systems for the cosmic ray test.

3 sMDT Base Chamber Construction on Granite Table

This section describes the assembly of the base chamber on the granite table using the jiggig described in Section 2 as well as measurements of the chamber mechanical precision done on the granite table after chamber assembly.

3.1 Spacer frame and in-plane alignment system assembly

The spacer frame parts are first cleaned with IPA and then are assembled with the in-plane devices and tested before being glued to the chamber. The mechanical shape of the frame is determined

by the assembly jiggling while its flatness, referenced to the surface of the granite table, is checked with 25 micron shims.

In the spacer frame the optical devices used in the four RASNIK lines are installed as shown in figure 13. The LED+mask and CCDs are mounted on the end cross-bars of the spacer frame, and the lenses for each RASNIK line are mounted on the center cross-bar. Images are taken after spacer frame is assembled to certify that the hardware is fully functional. Final reference RASNIK measurements are taken after the chamber is fully assembled and still held by the precision combs.

3.2 Gluing an sMDT base chamber

The tubes that have passed the quality control tests (including straightness, wire tension, gas leak, and dark-current measurements [5]) are cleaned with IPA before chamber gluing. They are arranged in eight groups by layer and their barcode ID is recorded in the database together with their final positions on the chamber. In addition, the precision combs are also cleaned with IPA and the tube ground screws inserted into the dedicated holes in the combs. An sMDT chamber is then assembled by gluing eight tube layers and a spacer frame with the precision jiggging set up on the granite table. This sequence takes 5 days: two days to glue the bottom multi-layer, one day to glue the spacer frame and the first tube layer of the second multi-layer, and the last two days to glue the remaining three tube layers on the top multi-layer.

Tube layer gluing is carried out by two operators (as in figure 20) placing the tubes on precision combs with all endplug plastic insulators adjusted to touch the RO-side end comb, so that tubes are lined up to allow proper electronics RO card installation later on. The automatic glue-machine dispenses Araldite 2011⁹ glue dots at 11 equidistant positions in each groove between the tubes.

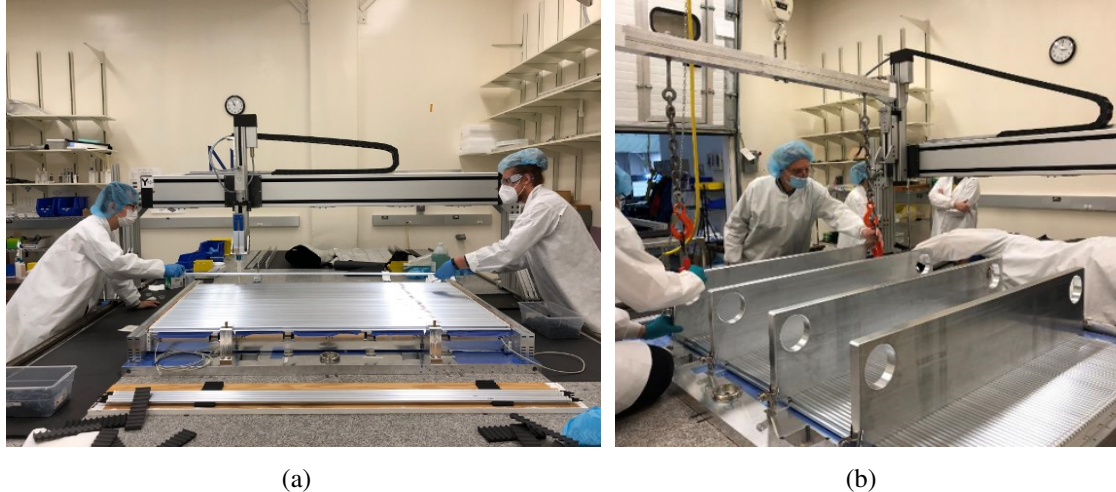


Figure 20: (a) Two operators are placing a tube on the comb following the automatic glue dispenser on the lower layer of the tubes. (b) Weights on tube layers after gluing.

The pre-assembled spacer frame is glued between the two multi-layers (MLs) of a chamber using DP190¹⁰ epoxy. The glue is dispensed on the top of the bottom ML tubes in a pattern following

⁹<https://krayden.com/technical-data-sheet/huntsman-araldite-2011-technical-data-sheet/>

¹⁰<https://multimedia.3m.com/mws/media/1235570O/dp190-scotch-weld-technical-data-sheet.pdf>

the spacer frame extrusion profile. Four temporary combs are placed on top of the bottom ML to help constrain the tube positions when the first tube layer of the top ML is placed on the two end combs and glued on the spacer bars.

After a layer of tubes is glued with the lower assembly combs, the next level of combs are screwed on the top of the former one on both sides with a torque of 7.5 Nm for each screw.

After the tubes are glued on the combs each day, 4 weights, each with the bottom side machined to reproduce a tube layer half-cylinder profile, are placed on top of the tube layer while supported on precision riser blocks, as shown in figure 20(b). The riser blocks set both the height and the lateral location of the weights, and are also used to prevent the outermost tube from bowing out. After the glue cures overnight, the weights are removed, and the ground-screws pre-loaded on comb layers 2, 3, 4, 6, 7, and 8 (counting from the bottom) are driven into the gap between the tubes.

3.3 Installation of the platforms and the chamber supporting structure

The ATLAS Muon spectrometer utilizes two types alignment sensors to determine the relative position of each chamber. The Axial-Praxial (AP) alignment system uses RASNIK sensors, and the CCC alignment system using SacCam sensors [3]. The AP system requires four platforms on each chamber, and the CCC system requires 1 or 2 platforms on selected chambers. Each chamber also utilizes two magnetic field sensors, which require two B-sensor platforms on each chamber. The location of each platform must be known to better than 30 μm , and the platforms must be glued on the chamber within 200 μm (500 μm in the case of the B-sensor platforms) of their target positions. The installation process of the plates and support structures takes two days: one day to glue the AP plates, and another day to glue the platforms for the CCC alignment and the B-field sensors, as well as the chamber support structures.

The AP-plates installation jigging was described in Section 2.5. The FARO-arm is mounted on the base cross-bar of the chamber jigging and used to set up the coordinate system for the two AP-plates' installation on the same side. The FARO-arm local coordinate system is defined by three perpendicular surfaces: the granite table, the side surface of the base cross bar, and the outside surface of the RO side end comb. The normal directions to these three planes form the coordinate axes (X, Y, Z). The intersection point of three surfaces determine the origin of the FARO-arm coordinate system. The cylinder centers of the top layer end combs are measured using FARO-arm to define the line of the first wire in this coordinate system. The FARO-arm measures then the 3D distances of an AP plate relative to the tube RO endplug surface (X), to the granite surface (Y), and to the first (or last) wire (Z), shown in figure 21.

Placing the AP-plates in correct positions is critical, since the assembly plate jigging (described in Section 2.5) relies on the AP plates to set the position of for B-field and CCC platforms. Multiple measurements with the FARO-arm and adjustments of the set screws are made for each AP plate before gluing to ensure the AP plate position is within the tolerances. DP490¹¹ epoxy is applied to the top layer of the tubes to bind each AP-plate, then a new set of measurements is taken and further adjustment of the AP plate position is performed if needed. The final position of the AP plates is measured after the glue has cured.

¹¹<https://multimedia.3m.com/mws/media/827900/dp490-scotch-weld-tm-adhesive.pdf>

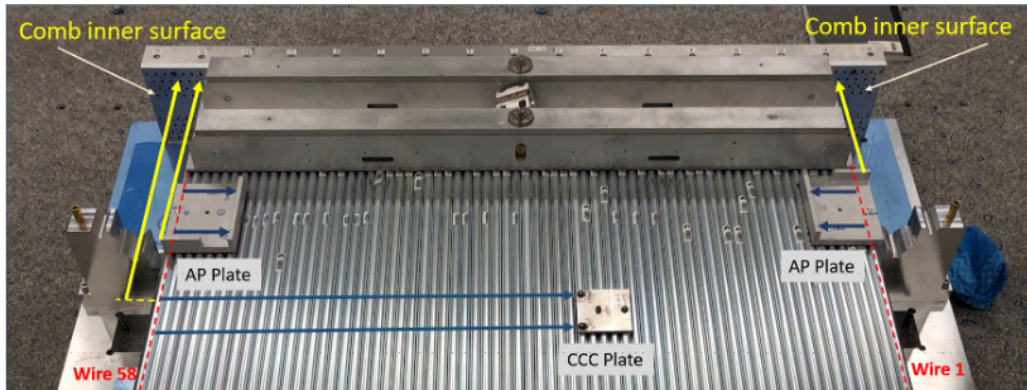


Figure 21: AP and CCC plates on top of the chamber. The blue and yellow arrows indicate the measurement points relative to the reference wires (in red) and the inner RO comb surface.

The CCC and B-sensor plates are mounted on the assembly plate and glued on to the chamber after the AP-plate glue is set. Figure 22(a) shows applying glue on a B-sensor plate which is mounted on the assembly plate prior to gluing on chamber. Figure 22(b) and (c) show lowering the assembly plate on top of the chamber, and checking that the assembly plate blocks are correctly positioned on the AP-plates.

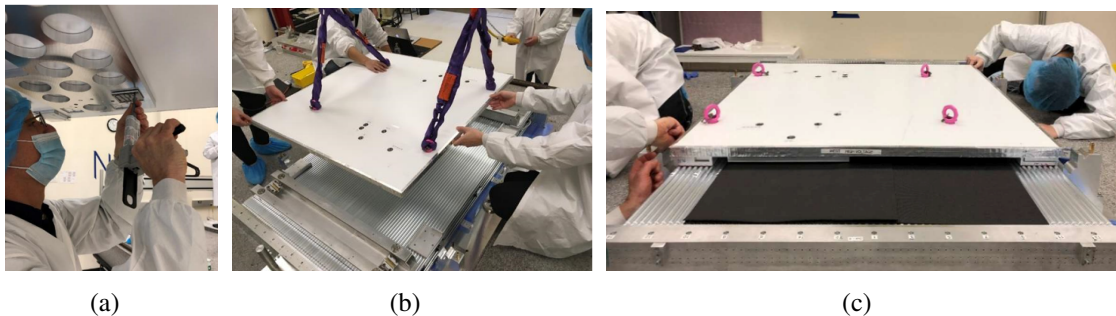


Figure 22: (a) Glue being applied to B-field and CCC-plates on the assembly plate; (b) assembly plate being placed on the AP-plates; (c) check of the assembly plate alignment with the AP-plates on chamber.

The chamber support structures (one can be seen in figure 21 clearly) contain the rail support bearings. Three kinematic mounting points, required for the chamber installation in the ATLAS experiment, are located in these structures. A 150 micron thick insulating tape is applied on the bottom side of the two support structures after they have been cleaned using IPA. DP190 glue is dispensed by the automatic glue machine on to the top of the tube layer matching the position and profile of each support structure. Two gauge blocks set the position of each support structure relative to the end-comb positions, and one common gauge block is used to set the position of the ends of the support structure relative to the first and last tubes.

3.4 Measurements of the base chamber mechanical precision

The chamber mechanical precision is measured by the 3D positions of the tubes and platforms, using the height gauge and the FARO-arm on the granite table, respectively. The platform positions are first measured while the chamber is still held by the precision combs. Next, the precision combs are removed, except the base combs and the tube positions are measured with the height gauge. The in-plane system RASNIK lines are also read out to record the base-line measurements of the chamber shape.

3.4.1 Platform position measurements

The platform positions are measured by the FARO-arm using the coordinates described in Section 3.3. Several distances corresponding to reference points, as indicated by the arrows shown in figure 21, are measured on the three perpendicular surfaces of each AP and B-field platform to determine their 3D positions relative to the reference positions. Each FARO-arm measured distance is compared with its nominal value and the deviation from the target value is calculated.

Figure 23 shows the measured AP-plate position offsets (in X, Y, Z) from the targets for the first 30 sMDT chambers built at UM. All AP-plates are placed well within the specified 200 microns maximum deviation from the nominal position. Similar results are obtained for B-field sensor positions, where the maximum tolerance is 500 microns.

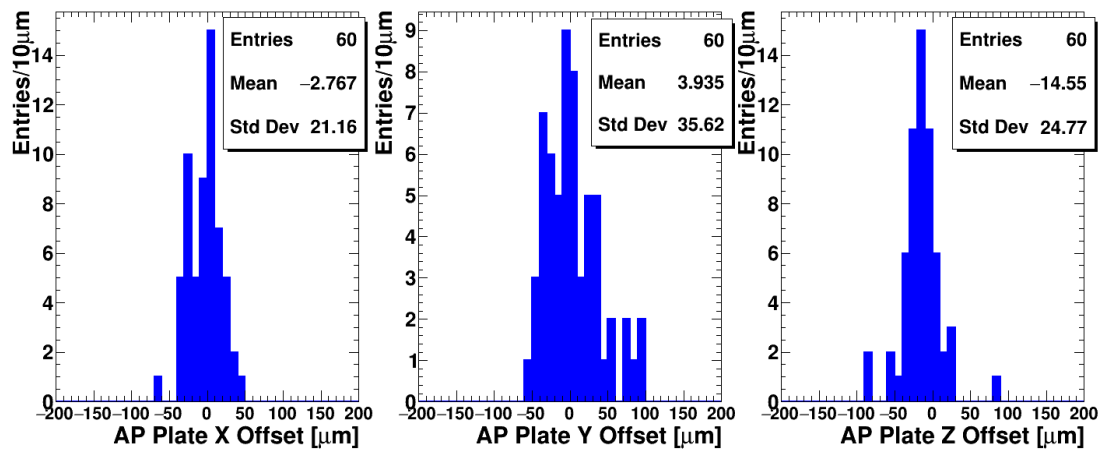


Figure 23: RO and HV AP plate position offset in X, Y, and Z from target values for the first 30 UM sMDT chambers.

In the case of the CCC-plates, an 8 mm precision sphere in a precision conical socket is measured to determine the center position of the plate. A small clamping arm, as shown in figure 24(a), was designed to hold the sphere rigidly allowing the FARO-arm probe to sample the surface of the sphere to perform this measurement. Figure 24(b) plots the deviation of the CCC sphere center X, Y, Z from to the target positions. Note that, by design, not all the chambers are instrumented with CCC platforms and installation jiggling was changed after building the first 8 BIS1 chambers. All CCC plates were installed at the target positions within the required accuracy of 200 microns, except for the Y-coordinates for a few early chambers which were out of the tolerance by a maximum of 47 µm.

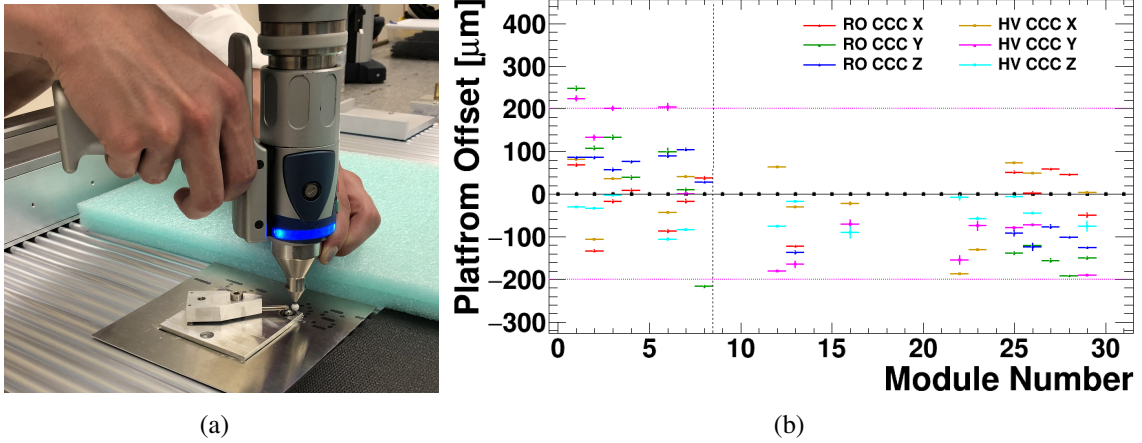


Figure 24: (a) A small clamping arm was devised to hold the sphere rigidly while the CCC plate is measured with the FARO-arm spherical probe; (b) Measured X, Y, and Z offsets of the CCC plate positions relative to target values for the first 30 UM sMDT chambers. The vertical black line indicates when the assembly plate was changed.

3.4.2 Tube position measurements

The tube height relative to the granite table surface is measured via the precision endplug cylinder surfaces using the height gauge with a flat probe, as shown in figure 25(a). Before the measurements

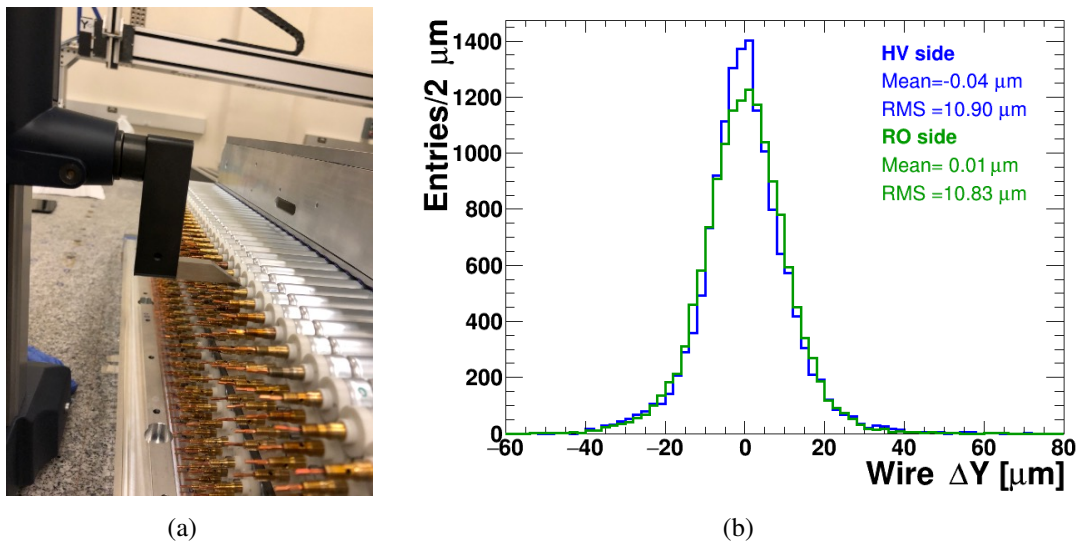


Figure 25: (a) Tube height measured on the endplug precision cylinders with a height gauge. (b) Histograms of the wire height offset from the layer mean for the first 30 UM sMDT chambers.

the granite surface used for the measurement is cleaned. The flat probe is frequently checked and tuned with a precision block to be parallel to the granite table. The zero of the height gauge is set before starting the measurement at a specific location on the granite surface and re-checked if an abnormal value is measured.

The histograms in figure 25(b) show the tube height deviations from the average in each tube layer for both the HV and RO sides. The RMS of these distributions is below 11 microns indicating the level of flatness of all the tube layers. The average height of each tube layer is recorded for both RO and HV sides of the chamber, from which the Y-pitch (vertical) of the tube layers and the spacer frame are determined. Figure 26 shows all the tube layer Y-pitch deviation from the nominal value for each built module.

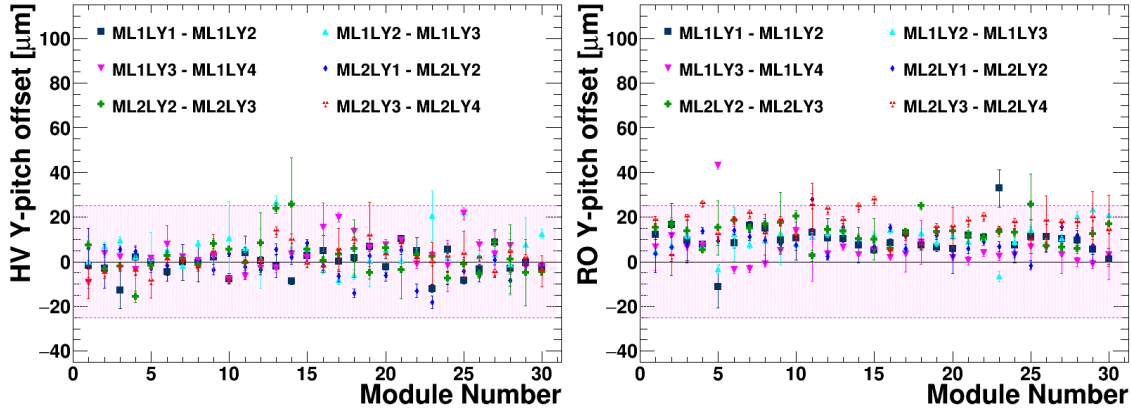


Figure 26: Tube layer pitch offset respect to the nominal value (13.077 cm) measured on both RO and HV sides for the first 30 sMDT chambers built at UM. A black zero line and a pink band of ± 25 microns are added to guide the eye.

The specified distance between the two multi-layers is 45.600 mm. The distribution of the spacer frame distances is shown in figure 27. The separation between the two multi-layers was found to be systematically lower than the target value for the first 20 chambers. Subsequent chambers were given an additional 50 micron mylar tape on the spacer frame cross-bars to increase the spacer frame distance to match the specification.

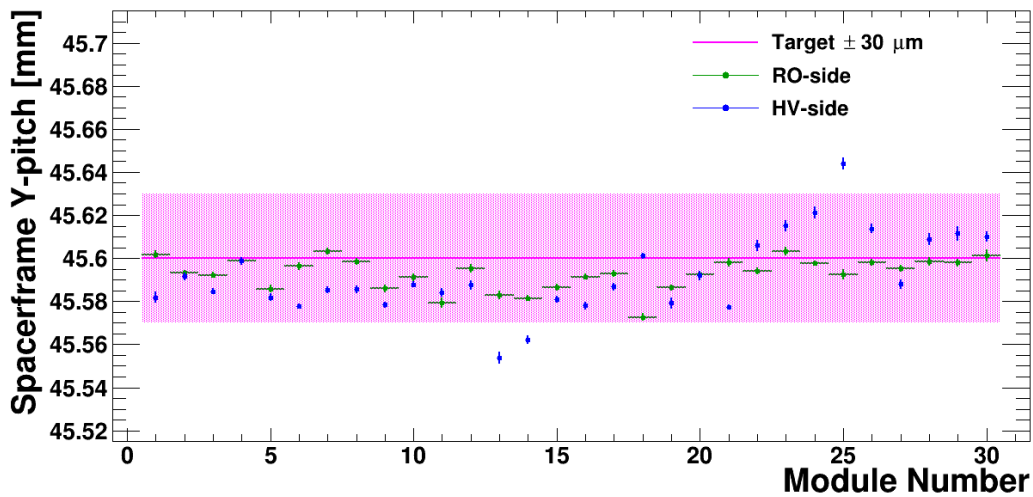


Figure 27: Spacer frame Y-pitch measurements for both RO and HV side for the first 30 sMDTs built at UM. The pink line is at the nominal value of 45.600 mm.

3.4.3 Chamber shape deformation measurements

The reference RASNIK measurement is made at the end of the construction while the chamber is still in the jiggging on the granite table. The chamber is then removed from the granite table and mounted on a rotation cart. On the rotation cart RASNIK measurements are taken at 22.5° intervals from which the granite reference values are subtracted to show the deformation of the chamber as it is rotated through 360° .

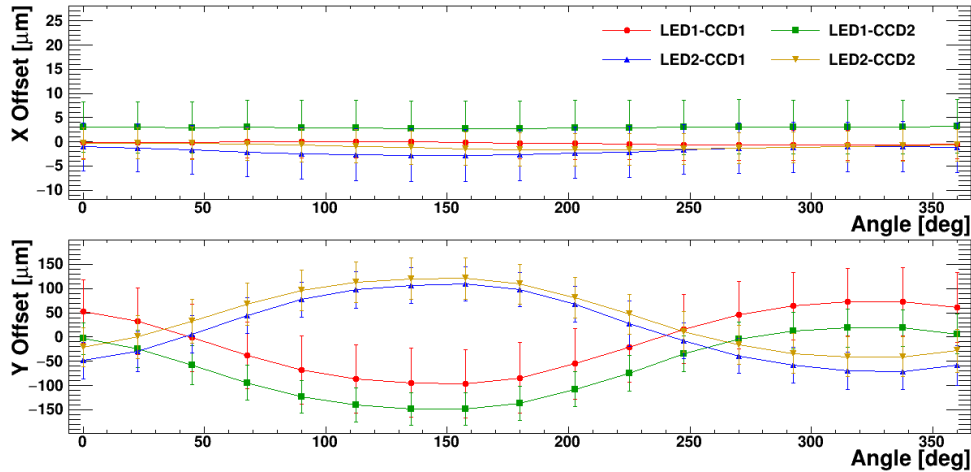


Figure 28: RASNIK measurements in chamber coordinates X (top) and Y (bottom) for all four RASNIK lines as the chamber is rotated through 360° . The data points value is the averages over the first 30 modules built at UM, while the error is the standard deviation of these measurements.

Figure 28 shows the result of these measurements for the first 30 sMDT chambers as deformation in the X and Y directions for all four LED-CCD RASNIK lines. The X direction is transverse to the layer of tubes (local XZ-plane) and the chamber is very stiff along this axis, hence there is very little deflection (a few microns) over 360° . The Y direction is perpendicular to the planes of tubes, and much more affected by gravity, hence the deflection is larger with a typical peak-to-peak variation of roughly 0.2 mm. These results, besides confirming the functionality of the system after the cabling to the readout panel, show that the optical in-plane devices cover a range of deformation of several hundredths of a millimeter.

4 Chamber Services Installation and Testing

The chamber services are installed when the chamber is on the rotation cart. The services installed are: temperature sensors, ground foil, gas manifolds, hedgehog electronics cards, Faraday cages, and ground straps. As soon as the chamber is removed from the jiggging all endplugs are covered with protective caps to keep dust from entering the tubes.

Temperature sensors, together with their readout cables, are glued in twelve positions on the chamber surface: six on the bottom surface and six on the top tube layer. Thermal contact between temperature sensors and tubes is made with thermal paste epoxy. All temperature sensor cables are routed to the top surface of the chamber through a hole in the support structure at the RO side, seen in figure 2(a). The RASNIK cables for in-plane system control and readout are also routed

along the top surface. A readout panel is built and installed on the RO side support structure of the chamber for connection to both the temperature sensor cables and RASNIK cables. A perforated foil is wrapped over each end of the chamber, providing common ground connections from the tube walls to each RO and HV hedgehog card. This foil becomes the internal wall of the Faraday cage that contains the electronics. Ground pins are screwed to the grounding anchors (installed during the gluing operations) and tightened up against this foil. These pins are installed after installation of the gas system, and before the hedgehog cards are installed.

4.1 Gas-bar assembly, cleaning, and installation on chamber

The sMDT gas distribution system uses molded plastic parts, shown in figure 29(a), which plug together in sets of 4 (to feed in series 4 tubes in a vertical stack across the 4 tube layers in a ML). On both sides of a ML either 58 or 70 of such stacks are connected to two gas-bars for parallel gas flow in and out of each ML. Gas input and output are at opposite corners to balance the impedance for uniform gas flow through all tubes.

All gas fittings are first ultrasonically cleaned with IPA, which is the only lubricant used during assembly. Each gas-bar is also ultrasonically cleaned in a bath of de-ionized water. After drying, each bar is wiped down with IPA. The inside length of the bar is then cleaned out using air pressure. Each bar is again wiped down with IPA.

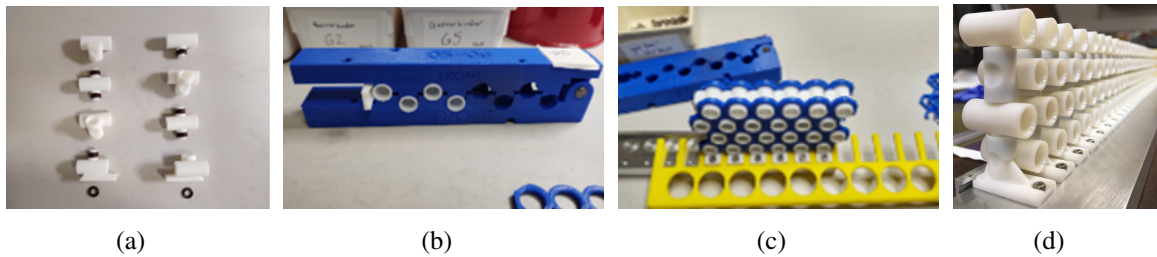


Figure 29: Gas-bar components and assembly: (a) Molded plastic gas fittings with o-rings form stacks of 4 (two different kinds); (b) blue 3-D printed jigging pre-aligns the 4 pieces of a stack; (c) stacks being mounted on a gas-bar manifold using more 3-D printed jigging parts to aid in alignment; (d) a gas-bar manifold with installed stacks, ready to be mounted on a chamber.

Each stack of 4 fittings is assembled using double o-rings between components. A sandwich jig, shown in figure 29(b) is used to align components for assembly. The sandwich jig and several other tools were made with a 3D printer to simplify gas-bar assembly (see figure 29(c)). Gas stacks are attached with M2.5X6 screws to the gas-bar with an o-ring in between each stack and the gas manifold. Different gas-bar configurations are made for the two sides of the chamber. Completed gas-bars are stored in lint-free bags prior to installation on chamber.

The gas-bar cleaning process was modified partway through chamber production because it was found that metal pieces left from the machining process could block a gas hole. This problem was found during cosmic ray testing where it was seen that some sets of 4 tubes connected to the same stack showed low efficiencies. To investigate this problem, the electronics and gas-bar were removed from the chamber. Further inspection revealed that small circular metal chips left over from hole drilling were blocking the holes in the gas-bar. The affected chambers had to have

electronics and gas-bar removed and the gas-bar carefully inspected for chips and re-cleaned. After reassembly, the tube efficiency was restored to normal values. The gas-bar cleaning procedure was subsequently modified to include the poking of each gas-bar hole to remove any metal fragments. Since this procedure was adopted no further issues with low efficiency stacks have been observed.

Figure 30 shows the gas-bar installation on a chamber. The ground foil is first laid and held by ground screw nuts onto the chamber. Each gas-bar is inserted into all the tube endplugs simultaneously using multiple special brass tools and three specially designed jiggging clamps (see figure 30(a)). O-rings, after ultrasonic cleaning with IPA, are placed onto the signal caps. Each

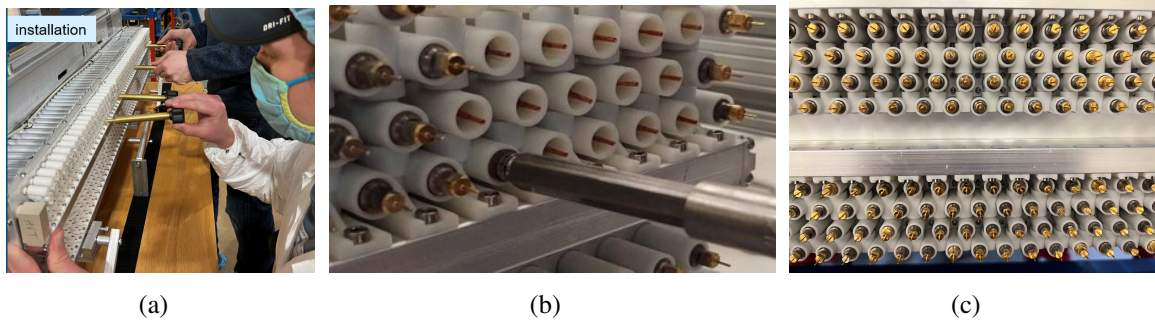


Figure 30: Gas-bar installation on a chamber: (a) fitting a pre-assembled gas-bar on the top ML of a chamber. The brass tools are used to make sure that all gas fittings are fully seated on their corresponding endplugs before beginning to install o-rings. The same tools are used to force an o-ring over the endplug precision surface where it is compressed by the gas fitting; (b) after the back o-ring is in place the signal-cap, which holds the outer o-ring, is screwed onto the endplug. The signal-cap has cross drilled holes which allow the gas from the fitting to enter the endplug and the tube body; (c) Two multi-layers with gas-bars and signal-caps installed.

signal cap is inserted into each gas connector using a special driver shown in figure 30(b). Complete gas-bar installation on both multi-layers on one side of a chamber is shown in figure 30(c).

The gas-bars are connected to an on-chamber gas distribution system using Swagelock fittings and valves connect the gas-bars as shown in figure 31. A high precision gas pressure gauge is temporarily connected to the gas system for chamber pressure measurements. The temperature of the chamber is monitored with 12 temperature sensors distributed on both sides of the chamber and readout through the patch panel shown in the picture.

4.2 Front-end electronics installation

The schematic of the electrical connections to an MDT drift tube is shown in figure 32. For an sMDT tube, the 383 Ω resistor in the HV side, shown in the figure, is replaced with a 330 Ω resistor. The RO and HV hedgehog (HH) cards consist mainly of passive components and mount directly on the signal and grounds via sockets on the cards.

There are two configurations of the HH and RO cards. One type has 24 channels with configuration of 4 \times 6 to span the 4 layers of a ML, 6 tubes wide. The other has 20 channels with configuration of 4 \times 5, which is installed on the ends of each ML. A total of 20 (16) 4 \times 6 cards plus

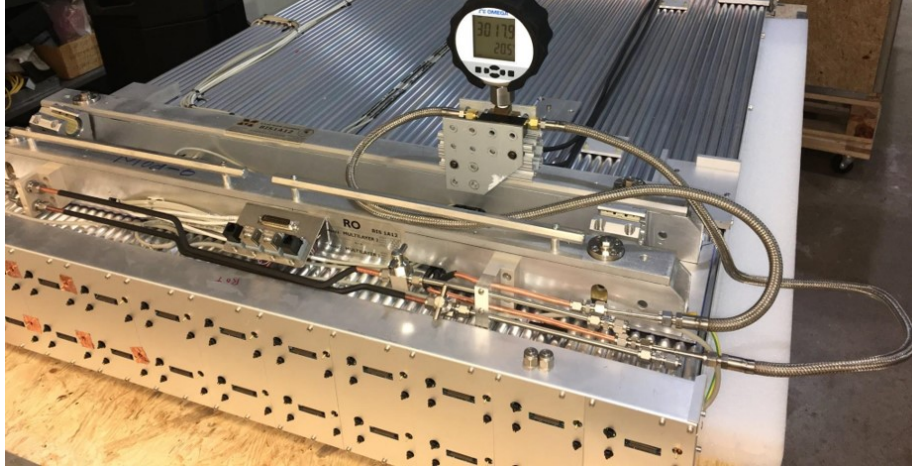


Figure 31: Completing the on-chamber gas system are 6 mm stainless steel and copper tubing pieces, Swagelok valves and fittings which connect the gas-bars to external supply lines. A high precision gas pressure gauge is here connected for the gas leak test, and the RO Faraday cage is already installed.

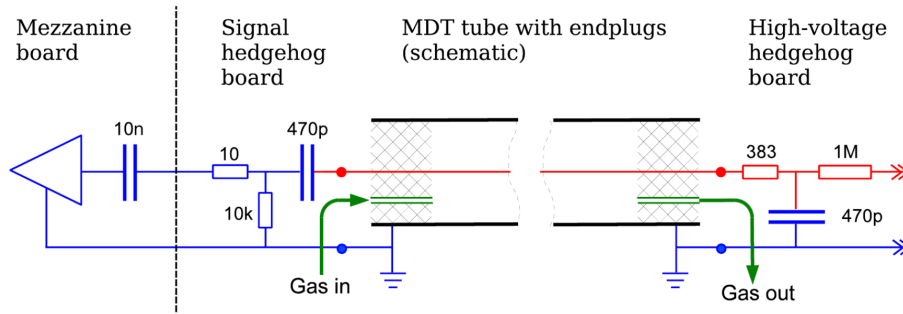


Figure 32: Electrical connections to an MDT drift tube [10]. Resistors values are in ohms (Ω). For an sMDT tube, the 383 Ω resistor is replaced with a 330 Ω resistor.

4 4×5 cards are installed in the BIS1 (BIS2-6) chambers. HV is distributed through four pairs of the input HV and ground cables. The HV HH cards are chain interconnected via PCB jumpers.

Faraday cages (FC) are installed around the HH cards to reduce noise. Two HV distribution boxes are mounted on top of the FC and distribution cables are routed through two holes of the FC. The FC on the RO side has the mezzanine cable connection holes to allow mounting the mezzanine cards to read out the chamber signals. The mezzanine cards hold the active components of the front-end electronics, the amplifier and time-to-digital converter chips.

4.3 Chamber gas tightness measurement

The ATLAS upper limit of the leak rate is $1 \times 10^{-5} [\text{mbar liter/s}] \times (2 N_{\text{tube}})$, where $2 N_{\text{tube}}$ denotes total number of endplugs included in the measurement. The tube gas volume is $V(\text{tube}) \approx 250 \text{cm}^3$, therefore the volume of each ML is $V_{\text{ML}} = N_{\text{tube}} \times 250 \text{cm}^3$. Using this information, the upper limit of the chamber leak rate can be converted to a limit on the chamber pressure drop per hour in the

measurements, which is 0.288 mbar/hour for a ML of an sMDT chamber.

Since the chamber pressure depends on gas temperature, the measured pressure change (ΔP) over time interval (Δt) must be corrected to be compared to the specified leak rate limit. The chamber normalized leak rate is determined by

$$\left(\frac{\Delta P}{\Delta t}\right)_{norm} = \frac{\Delta P_{corr}}{\Delta t}$$

where ΔP_{corr} is the change in pressure corrected with the temperature variation over a time interval Δt , calculated as:

$$\Delta P_{corr} = P_f \frac{T_{ref}}{T_f} - P_i \frac{T_{ref}}{T_i}$$

where P_i , P_f , T_i , T_f are initial and final pressure and temperature, and $T_{ref} = 293.15^\circ$ K is used as reference temperature.

The chamber gas output valves are connected to a pressure gauge (see figure 31), which can monitor each ML gas pressure. The chamber is pressurized with Helium gas, then a Helium sniffer is used to detect leaks from connection points and/or individual tubes. Most leaks can be fixed quickly by replacement of o-rings, gas stacks, or signal caps. A few tubes have developed leaks which cannot be fixed. For these, the wire is removed, the end plugs sealed to isolate the tube from the gas system, and the signal caps modified to isolate the tube from both the HV and RO electronics.

The final leak rate measurement is performed with all HH cards and the Faraday cages installed. The resistance of all 12 temperature sensors is measured in Ohms, converted into degrees Celsius and averaged for each ML to correct the initial and final chamber ML pressures readout during the leak test, which check the pressure drop as a function of time. The measured ML leak rates of the first 30 sMDT chambers built at UM are shown in figure 33. The pink dashed-line in the plot indicates the upper limit, and blue (red) triangles are the measured leak rates for ML1 (ML2) of produced chambers at UM, all well below the allowed upper limit.

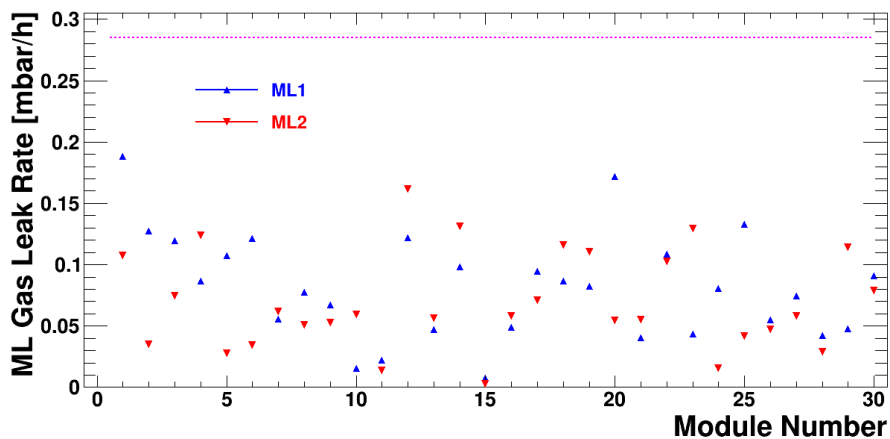


Figure 33: Multi-layer gas leak rate of the first 30 sMDT chambers built at UM. The dashed line represents the ATLAS maximum acceptable gas leak rate.

4.4 Ground cable connections

The chamber grounding follows a "star" design that avoids ground-loops. The schematic of the ground connectivity is shown in figure 34, where the pictures show how the grounding cables (in green color) connect the gar-bars, chamber side-panels, and the chamber support structures.

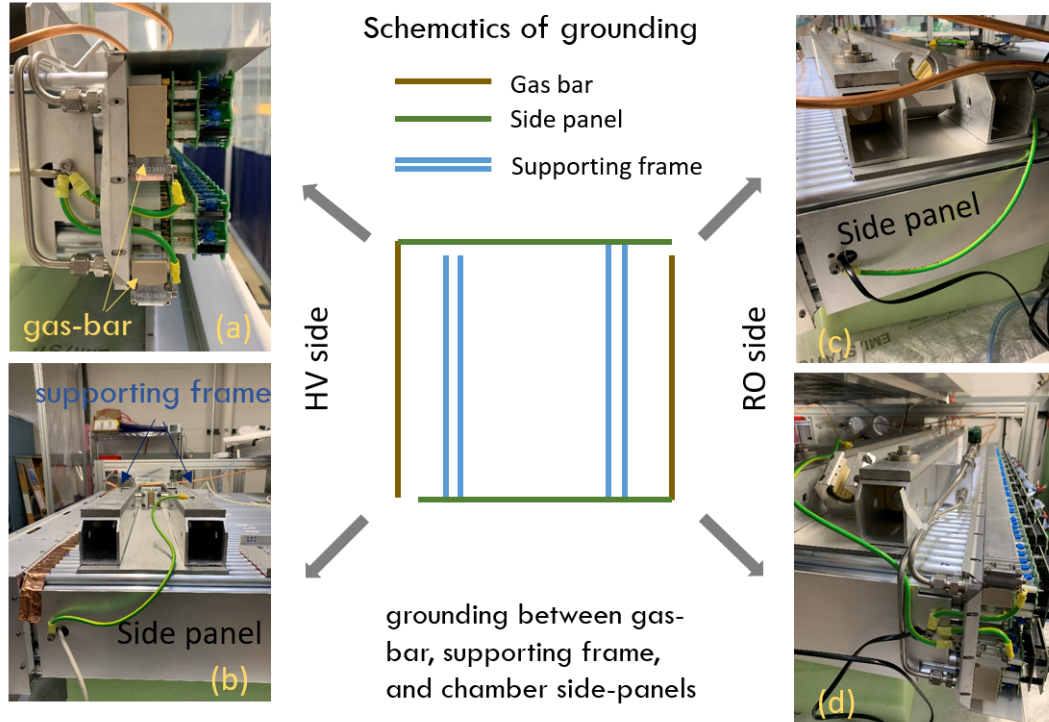


Figure 34: Grounding cable connections schematics. Pictures show detailed connections to the gas-bar (a), side-panel (b), support structure (c), and between the gas-bar and the support structure.

5 Electronics and Cosmic Ray Test

The final QA/QC tests include measurements of the noise level and efficiency of each tube, as well as the chamber tracking efficiency and resolution. These tests are carried out in the cosmic ray test station which has been described in Section 2.6.2.

Each chamber runs for a minimum of 24 hours at the operating HV (+2730 V) to ensure that the current drawn is at a level below 2 nA times number of tubes. Tubes which draw excessive current are individually treated with negative HV (up to -3 kV) for about one hour to reduce the current below the 2 nA limit. Finally, the readout mezzanine cards are installed on top of the RO HH cards. One mezzanine card contains a board with three ASD (Amplifier/Shaper/Discriminator) ASIC chips, each with 8 channels, and another board with one 24 channels high-performance time-to-digital converter (HPTDC) chip on top of the ASD board. Figure 35(a) shows a mezzanine card installed on a chamber. Two Chamber Service Modules (CSMs) are used to multiplex the readout from all the HPTDCs of a chamber (each CSM can multiplex up to 18 HPTDCs). The DAQ system

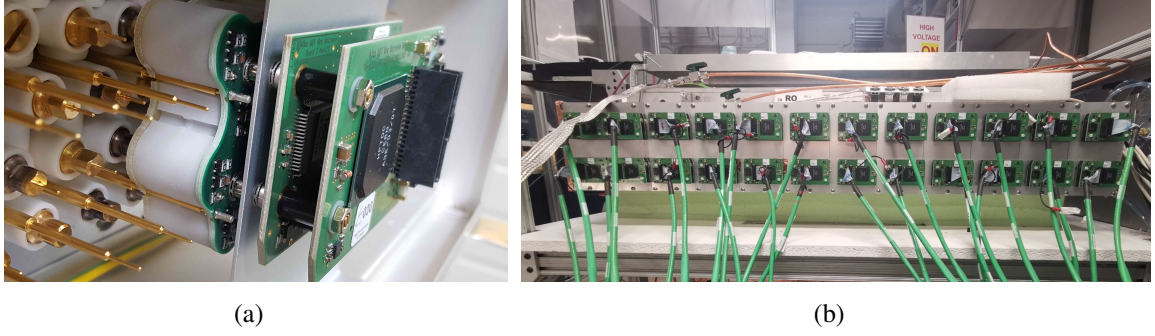


Figure 35: (a) A 24 channel RO HH and mezzanine card mounted on a sMDT chamber; (b) 24 front-end electronics cards on a BIS1 chamber RO side.

with a scintillator trigger and the online monitoring system are connected to the test chamber for measurements. An offline analysis program (detailed description of the algorithms in [11]) was developed to measure the performance of each tube and ultimately the efficiency and the resolution.

5.1 Noise rate measurements

Each tube noise rate is measured in a series of data runs at different readout thresholds with both HV-off and HV-on (at the nominal working voltage of +2730 V). A 10 KHz pulse-generator is used as trigger to read out noise hits. The noise rate can be calculated based on the recorded number of hits and the number of triggers during the data taking period (typically $\Delta t = 10$ minutes) as:

$$\text{Noise rate} = \frac{N_{hits}}{N_{trigger}} \times \text{time}_{window} ,$$

where time_{window} ($1.55 \mu\text{s}$) is the HPTDC readout time window; N_{hit} is the number of hits in each channel recorded in the test time Δt , and $N_{trigger} = 10 \text{ KHz} \times \Delta t$.

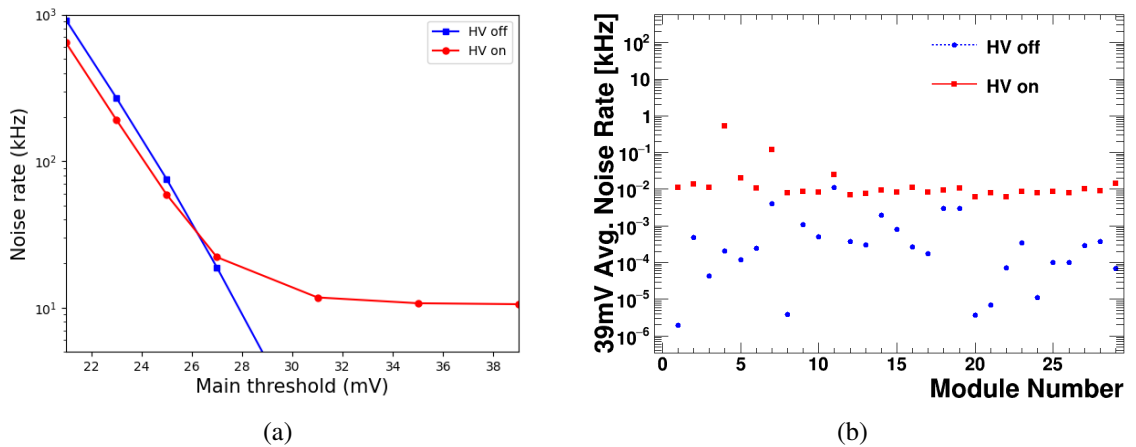


Figure 36: (a) Noise rate vs. threshold for a representative sMDT chamber. (b) Chamber average noise rate measured at 39 mV threshold for the first 30 modules.

The measured noise rate vs. ASD threshold for a representative sMDT chamber built at UM is shown in figure 36(a). When the readout threshold is larger than ~ 30 mV, the chamber hit rate is dominated by the cosmic rays, as seen from the red curve measured with HV-on. The specification of the maximum tube noise rate is 500 Hz at the readout threshold of 39 mV. Figure 36(b) shows the average noise rate measured at 39 mV threshold for the first 30 sMDT built at UM, all well below 500 Hz, except Module-4 with noise rate close to the specification in the HV-on measurement. This chamber will be closely evaluated again during the final commissioning phase at CERN.

5.2 Tube spectra from cosmic ray data

Each tube's response to charged particles is tested with cosmic rays. Figure 37 shows typical (a) time (TDC) and (b) charge (ADC) spectra for the hits of a tube on a representative sMDT chamber together with their fits (described in [11]). Both the leading and trailing edge of the TDC distribution are fit with a Fermi-Dirac function in order to get the time offset (T_0) and the maximum time T_{Max} . The ADC distribution is fit with a skew normal function.

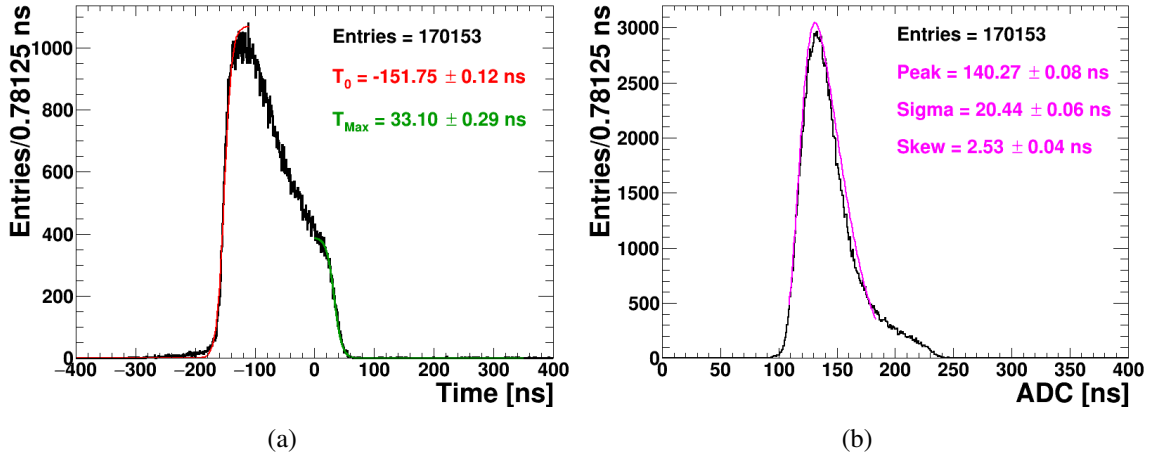


Figure 37: Distributions of cosmic ray hits recorded by a typical tube: (a) time, (b) charge.

The measured hit drift time, calculated as the difference between the hit time and the T_0 , is then corrected with the time-slew correction using the charge information. The time-slew effects are due to the jitter introduced by different times of crossing the ASD threshold by different amplitude signals.

5.3 Tube and chamber efficiencies

Figure 38(a) shows an example of the chamber response uniformity based on the number of hits per tube in the cosmic ray run.

The definitions of efficiency rely on having successfully reconstructed a track. A muon track is built starting from the sMDT hits for each triggered event by fitting the hits drift distances obtained from the (corrected) drift times via an $R(t)$ function. This time-to-space relationship is obtained with an auto-calibration program that converts the drift time to the drift distance through a procedure of minimizing the tracking residuals of all the collected muon tracks in a test run. An example of a cosmic ray muon track reconstructed in an sMDT chamber built at UM is shown in figure 38(b).

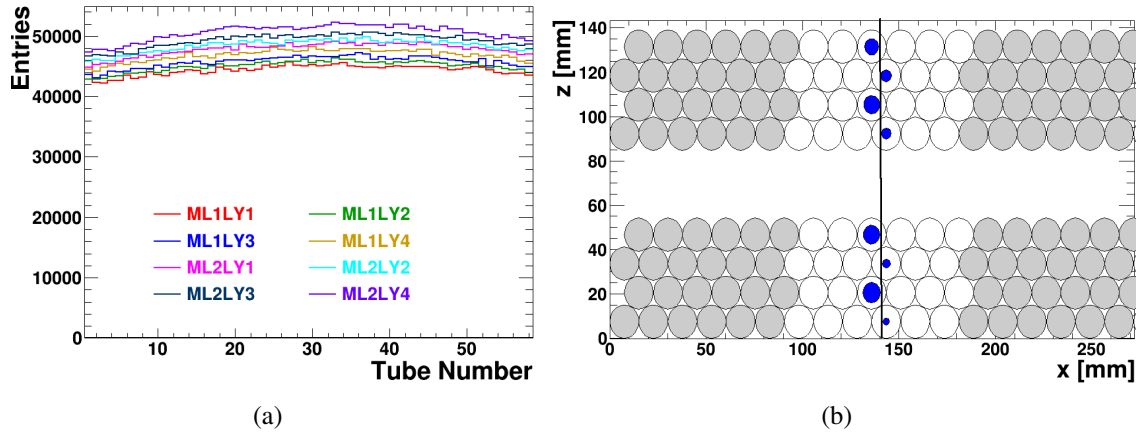


Figure 38: (a) Cosmic ray run hit map for the 8 tube layers as a function of the tube number for a representative sMDT chamber; (b) example of a track reconstructed in a sMDT chamber by a fit tangent to the drift circles (blue circles). Grey (white) circles are drift tubes read out by a different (the same) mezzanine card.

The tube efficiency is defined as the ratio between the number of hits recorded on a track passing through that tube and the number of reconstructed tracks passing through the gas-volume of that tube. Figure 39(a) shows this single tube detection efficiency, which is on average $99.02 \pm 0.01\%$ for the first 30 chambers built at UM.

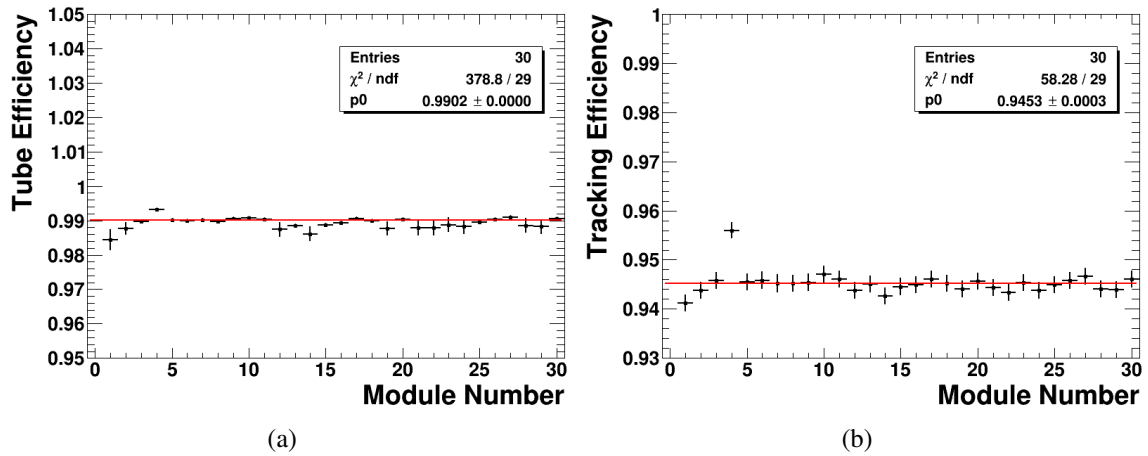


Figure 39: (a) Tube and (b) tracking efficiency for the first 30 sMDT chambers built at UM.

The tube layer efficiency is defined as the number of hits in that layer belonging to a track divided by the number of tracks passing through that layer. This latter efficiency includes the tube efficiency as well as the inefficiency of the tube walls and the space between tubes (dead regions). Figure 39(b) shows the tube layer efficiency averaged over a chamber (called tracking efficiency). The average tracking efficiency for each tube layer is $94.52 \pm 0.03\%$.

Out of the 14688 tubes of the first 30 UM sMDT chambers, 13 were lost due to wire slippage (insufficient crimping) or irreparable gas leaks (cracked endplug or improper endplug swaging).

5.4 Tracking resolution

The ATLAS muon spectrometer measures the momenta of muons by reconstructing the curvatures of their trajectories in the magnetic field, and thus the spatial tracking resolution will in turn determine the resolution of the momentum measurement.

The single tube resolution is determined by fitting the reconstructed muon tracks and evaluating the residual distributions. The tracking residual is the difference $r_{\text{drift}} - r_{\text{fit}}$, where r_{drift} is the measured drift radius and r_{fit} is the radius obtained by the track fit. Two types of residuals are introduced, biased and unbiased. The biased one is the residual when the track is fit with all hits. The unbiased one is the tracking residual of a hit from a track reconstructed by removing that hit from the fit. Figure 40 shows the biased and unbiased residual distributions.

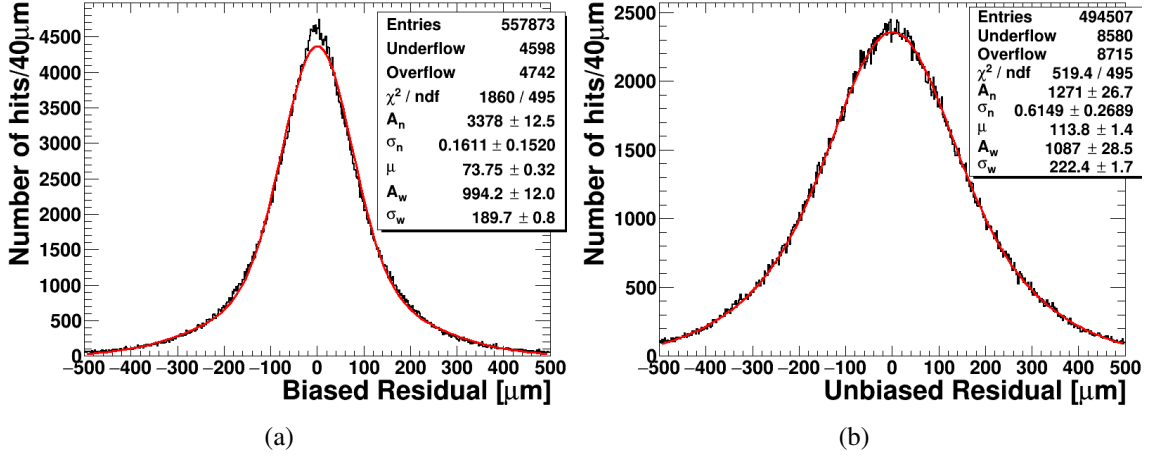


Figure 40: (a) Biased and (b) unbiased residual distribution for a representative sMDT chamber built at UM with a double Gaussian function fit.

A residual distributions is fitted with a double Gaussian function with common mean (see [12] for details) and the single wire resolution is defined as [13]:

$$\sigma_{\text{wire}} = \sqrt{\sigma_B \cdot \sigma_U} \quad (5.1)$$

where σ_B (σ_U) is the biased (unbiased) residual width calculated as amplitude weighted average of the two Gaussian components, narrow (n) and wide (w), of the fit:

$$\sigma_\alpha = \frac{A_n \cdot \sigma_n + A_w \cdot \sigma_w}{A_n + A_w}, \quad (\alpha = B, U). \quad (5.2)$$

The multiple Coulomb scattering effect on low energy cosmic ray muons are corrected when computing the resolution [11]. The single wire resolution vs. the tube radius for a representative sMDT chamber built at UM is shown in figure 41(a). The measured tracking resolution (integrated over all radii) for the first 30 chambers made at UM shown in figure 41(b), is $100 \pm 7 \mu\text{m}$ to be compared with the expected value of $106 \mu\text{m}$ [14]. The resolution of the constructed chambers is better than the specification because the expected value was estimated using the first generation of

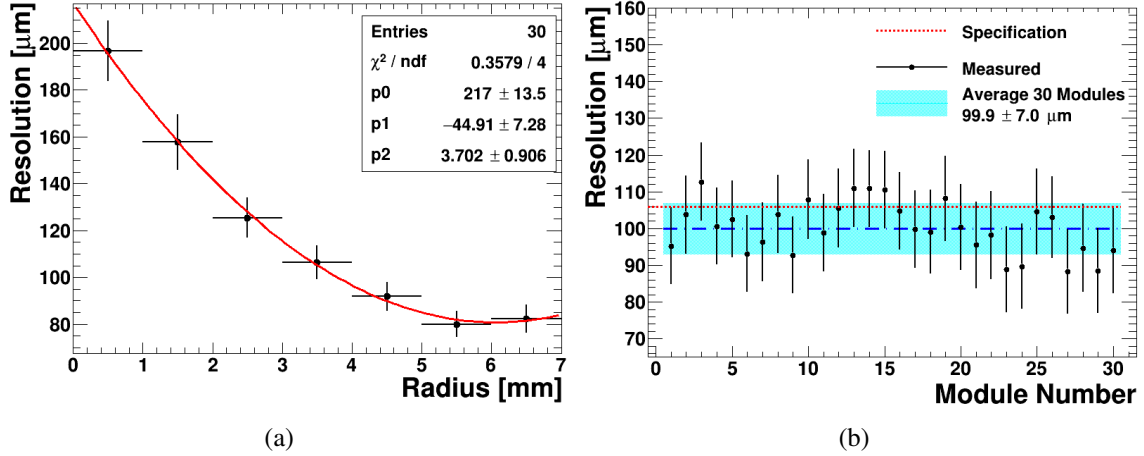


Figure 41: (a) Average resolution vs. radius of the 30 sMDT chamber built at UM. The errors are the standard deviations of the 30 data-point at that drift radius; (b) chamber resolution for the first 30 sMDT chamber built at UM.

the electronics (in particular the ASD-1), while the sMDT built at UM are tested with mezzanine cards instrumented with the final ASD-2 which has a higher gain.

All chambers constructed at UM so far meet the performance specifications both for tracking resolution and efficiency.

6 Database

All the information about each chamber construction precision measurements, gas tightness, and electronics tests as well as the overall performance are assembled into a local database, ready to be checked and/or displayed. The data from the various measurements and tests stations is usually saved in text files, either directly or after an initial decoding/analysis on the output data from a test station. This format of the local data storage allows converting to different databases (MS Access, MySQL, Oracle, JSON, ...) for the task. The most natural choice is a relational database, since all information to be saved is relative to many single units (as tubes, sensors, plates, tube-layers, multi-layers, ...), each one with a list of properties, test parameters and results: all data is correlated.

With the goal to store, quickly retrieve, and eventually show the data, a ROOT [15] based approach is used. C++ classes read each chamber (and corresponding tubes) data files and organize them into a (multiple) set of measurements with conditions and relative data into a *TTree* of the ROOT file. The main blocks of this *TTree* are described below.

Construction: Includes the IDs of the tubes, their locations on the chamber and the measurements of the tube heights relative to the granite table. From this data the average height of a tube layer is calculated and then each layer and spacer frame Y-pitch are determined. Also, the positions of all the platforms (AP, B-field, and CCC) glued on the chamber are recorded.

In-plane alignment: Stores the RASNIK system data from the final measurement on the granite table (the base-line measurements) and at different inclination angles on the rotation cart.

Gas leak rate: Saves the gas pressure for each chamber ML together with the temperature at different times to determine the gas leak rate.

Noise level: Retains the noise rate for each tube for HV-off and HV-on runs at 8 different ASD thresholds.

Electronics performances: Collects each tube efficiency together with its cosmic ray test TDC and ADC spectra, as well as the tracking efficiency, the chamber biased and unbiased hit residual distributions, the single wire resolution, and the resolution vs drift radius.

In all these ROOT-based DB *Trees*, the tube barcode ID is the primary key for retrieving information from the measurements on a tube, either as a single unit (wire tension, dark current, and so on, see [5]) or part of an assembled chamber (tube heights over the granite table surface, efficiency, resolution, and so on.) While filling the *Tree*, a set of standard plots for each test is automatically saved, ready to show trends and/or discrepancies between a chamber and all the others already tested or reference values. A dedicated set of files with common formats, which are followed by both Michigan and the MPI production sites, is prepared and uploaded to the CERN website¹² to share the results by both sites on the sMDT chamber production quality control. This common database on sMDT production will be used for future sMDT commissioning and operations in the ATLAS experiment.

7 Conclusion

With the elaborate infrastructure built at UM, 30 sMDT chambers have been constructed meeting the stringent precision and quality requirements. These chambers are all thoroughly tested with cosmic rays and achieve a single tube efficiency above 99%, and tracking resolution of $100 \pm 7 \mu\text{m}$.

There are three major steps in the chamber construction and certification (base chamber gluing, services installation, and final cosmic ray testing), each requiring 10 working days on average. The three steps are carried out in parallel in order to meet the production schedule.

Of the 30 chambers constructed at UM, the first batch of 24 chambers has already been delivered to CERN. 20 more chambers are still to be constructed at UM and will be delivered to CERN by the end of 2023. The final commissioning of all 50 Michigan chambers prior to installation on the ATLAS cavern is planned to begin in 2024 at CERN.

Acknowledgments

We would like to thank Hubert Kroha and Oliver Kortner (MPI), Rinat Fakhruddinov (IHEP, Protvino), Reinhard Schwienhorst (MSU), Tristan Du Pree (NIKHEF), Pierre-François Giraud (Saclay), and their team members for their close collaborations and valuable technical discussions. We also thank the UM ATLAS faculty, Jianming Qian and Shawn McKee for their strong support, and our undergraduate students, Tyler Coates, Kathryn Ream, Dylan Ponman, Saarthak Johri, and Yuxin Wan, for their great technical assistance.

This work was supported in part by the U.S. Department of Energy grant DE-SC0012704 and in part from the U.S. National Science Foundation PHY-1948993.

¹²<https://atlas-mdt-phase2-qc.web.cern.ch/>

Bibliography

- [1] ATLAS collaboration, *The ATLAS experiment at the CERN large hadron collider*, *JINST* **3** (2008) S08003.
- [2] ATLAS collaboration, T. Kawamoto, S. Vlachos, L. Pontecorvo, J. Dubbert, G. Mikenberg, P. Iengo et al., *New Small Wheel Technical Design Report*, CERN-LHCC-2013-006, ATLAS-TDR-020, <https://cds.cern.ch/record/1552862>.
- [3] ATLAS collaboration, *Technical Design Report for the Phase-II Upgrade of the ATLAS Muon Spectrometer*, CERN-LHCC-2017-017, <https://cds.cern.ch/record/2285580>.
- [4] B. Bittner and al., *Development of muon drift-tube detectors for high-luminosity upgrades of the large hadron collider*, *Nucl. Inst. & Meth. in Phys. Res. A* **617** (2010) 169 (2010) .
- [5] C. Wei, A. Chen, D. Amidei, N. Anderson, E. Carpenter, L. Cooperrider et al., *Construction and testing of smdt tubes at the university of michigan for the atlas muon spectrometer upgrade*, *Journal of Instrumentation*, <http://arxiv.org/abs/2209.03864> (Oct, 2022) .
- [6] M. Beker, G. Bobbink, B. Bouwens, N. Deelen, P. Duinker, J. van Eldik et al., *The rasnik 3-point optical alignment system*, *Journal of Instrumentation* **14** (aug, 2019) P08010–P08010.
- [7] J. Barriere and al., *The alignment system of the barrel part of atlas muon spectrometer*, *ATL-MUON-PUB-2008-007* .
- [8] R. Bitter, T. Mohiuddin and M. Nawrocki, *LabVIEW: Advanced programming techniques*. Crc Press, 2006.
- [9] Y. Guo, J. Wang, Y. Liang, X. Xiao, X. Hu, Q. An et al., *Design of a Time-to-Digital Converter ASIC and a mini-DAQ system for the Phase-2 upgrade of the ATLAS Monitored Drift Tube detector*, *Nucl. Instrum. Meth. A* **988** (2021) 164896.
- [10] Y. Arai and al., *Atlas muon drift tube electronics*, *JINST* **3** (2008) 0P9001.
- [11] K. Nelson, Y. Guo, D. Amidei and E. Diehl, *Performance of Michigan SMDT prototype chambers for the HL-LHC ATLAS muon detector upgrade*, *Journal of Instrumentation* **16** (Nov, 2021) P11027.
- [12] ATLAS collaboration, G. Aad et al., *Resolution of the ATLAS muon spectrometer monitored drift tubes in LHC Run 2*, *JINST* **14** (2019) P09011.
- [13] R. Carnegie, M. Dixit, J. Dubeau, D. Karlen, J.-P.Martin, H. Mes et al., *Resolution studies of cosmic ray tracks in a TPC with GEM readout*, *Nucl. Instrum. Meth. A* **538** (2005) 372–383.
- [14] H. Kroha, R. Fakhruddinov and A. Kozhin, *New High-Precision Drift-Tube Detectors for the ATLAS Muon Spectrometer*, *JINST* **12** 12.
- [15] R. Brun and F. Rademakers, *Root - an object oriented data analysis framework*, *Nucl. Inst. & Meth. in Phys. Res. A* **389** (1997) 81-86 (1996) .